Dear Editors,

We have revised the manuscript according to the recommendations of the reviewers. Below we will list the most important changes compared to the ESSDD version of the manuscript. A pdf manuscript created with LatexDiff is attached to this "Author's Response".

We have determined the sampling error and also examined the clear-sky bias of the TCWV data set. In addition, we have also investigated the extent to which filtering the row anomaly affects the TCWV data. This has significantly improved the characterisation of the OMI TCWV dataset (see Section 4 in the revised manuscript).

We describe in more detail our uncertainty assumptions for the different data sets for the intercomparison studies and document the comparisons with more descriptive/quantitative statistics. Moreover, we have also adjusted the Figures in accordance to the critique of Reviewer #1 and show the results of the ODR and PWLF regression in the same panel.

We would like to thank the referee for reviewing our manuscript. Below we reply to the issues raised by the referee, where
blue repeats the reviewer's comments,
black is used for our reply,
and green italics is used for modified text and new text added to the manuscript.

Review of manuscript essd-2021-319 entitled "A 16-year global climate data record of total column water vapour generated from OMI observations in the visible blue spectral range" by Christian Borger, Steffen Beirle, and Thomas Wagner.

General comments

This manuscript presents a total column water vapour (TCWV) data set derived from 16 years of OMI observations. The retrieval method was developed in a previous publication (Borger et al., AMT, 2020). It has been slightly improved in order to meet the long term stability requirements for a climate data record. The manuscript describes briefly the modified aspects of the retrieval algorithm and gives additional details on the data quality control applied for this specific purpose. The latter seems to reject a significant fraction of the raw data, although this number is not indicated. Most of the manuscript is devoted to a comparison/validation analysis of the OMI TCWV results with respect to satellite microwave radiometer data (SSM/I), reanalysis data (ECMWF's ERA5), and the ESA/CCI/CDR-2 water vapour product. The comparison results are fairly documented, including scatter plots, Hovmoeller diagrams and maps, although some synthetic statistics are missing (see the specific comments below). However, the conclusions sound far too optimistic to me, given the poor agreement found between the OMI data and the validation data. Especially, the large positive biases over land and near the coastlines in the tropics are striking and not sufficiently commented or explained. Two main reasons are hypothesized: too low land surface albedo and incorrect cloud information, both leading to an underestimation of the AMF. These paths should be further explored in order to achieved a more reliable product meeting the climate data quality requirements. Although it is shown that the results are improved when a special could mask is used, this is only an artificial way to improve the quality of the product.

Regarding the temporal stability, it is not clear how the significance of the global mean bias, RMSE, and trend differences are established. It seems to me that the numbers are beyond the limits usually required for water vapour climate data (e.g. an error of 0.1%/decade in the global mean TCWV trend represents nearly 20% of the signal). Moreover, the uncertainty due to different time and space sampling with the different reference products should also be quantified.
Many thanks for pointing out the GCOS requirements! For our value of 1.0%/decade we have followed the User Requirements of the ESA CCI WV (https://climate.esa.int/media/documents/Water_Vapour_cci_D1.1_URD_v3.0.pdf). If we understand correctly, the value of 0.3%/decade in the GCOS document refers to radiosonde measurements or their WVMR measurements (see requirement tables in Appendix 1 of the GCOS document suggested below in the Specific Comments). Please also note that the requirement mentioned refers to the global mean. However, we are also interested in regional trends, which usually have significantly higher magnitudes.
In addition, we determined the sampling error (and the clear-sky bias) and added the following text to the revised version:
Although satellite observations enable the analysis of trace gas concentrations on global scale, a fundamental problem is that typically a satellite measurement is only taken once a

day for one location. Furthermore, satellite measurements are usually only available under cloud-free conditions, especially in the visible or infrared spectral range and thus no continuous time series is guaranteed. Consequently, they cannot provide a complete picture of geophysical variability, which leads to sampling errors in the calculation of averaged values (e.g. monthly means).

Moreover, the question arises to what extent the limitation to cloud-free pixels influences the monthly averages determined from the OMI satellite measurements, i.e. whether in the OMI TCWV data set a so-called "clear-sky bias" exists. Gaffen and Elliott (1993) investigated this bias using radiosonde ascents and found that the TCWV is about 0-15% lower under cloud-free conditions than under cloudy conditions. Similarly, Sohn and Bennartz (2008) found a clear-sky bias between MERIS and AMSR-E of about 10%.

To estimate the sampling errors, we follow the methods of Xue et al. (2019) and Gleisner et al. (2020): we choose hourly-resolved ERA5 data with a spatial resolution of 0.25°x 0.25° as reference data and collocate the ERA5 data with OMI overpass times. These data are then resampled to the 1°x1° resolution of the OMI TCWV data set and the monthly averages are calculated (TCWV_sampled). We then take the complete, original ERA5 data, resample it to the same spatial resolution and calculate monthly means from this data as well (TCWV_true). The difference between the two data sets then represents the sampling error:

e_sampling = TCWV_sampled – TCWV_true (4)

With this definition, the sampling error summarises the uncertainties due to gaps in the swath, temporal differences or missing data (e.g. due to clouds) (Xue et al., 2019).

Figure 3 shows the annual mean absolute and relative sampling errors for the year 2006. Overall, it can be seen that most deviations are negative, i.e. the actual TCWV is underestimated. Regarding the absolute deviations, the strongest deviations can be seen in the area of storm-tracks in the mid-latitudes (e.g. North Atlantic) and the polar regions with values around -5 kg m-2. The smallest deviations are found in the quasi-permanent cloud-free regions in the subtropics. As expected, the relative differences increase from the equator towards the poles due to the decreasing TCWV values and reach values stronger than -30%.

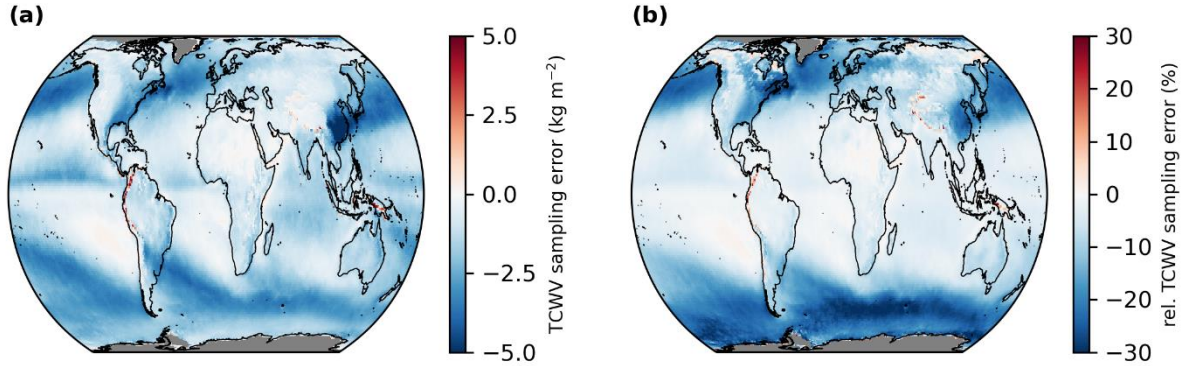

Figure 3. Global distributions of the mean sampling errors derived from monthly mean sampling differences for the time range January 2005 to December 2020. Panel (a) depicts absolute sampling error (i.e. "sampling) and Panel (b) relative sampling error (i.e. "sampling=TCWVtrue). Grid cells for which no data is available are coloured grey.

To investigate to what extent these deviations are related to the clear-sky bias, we proceed similarly to the calculation of the sampling error: we collocate the ERA5 data to the OMI overpass time and once apply a cloud filter (effective cloud fraction < 20%) and once not. Then we resample both data sets to 1°x 1° and calculate monthly means. The difference of both data sets then represents the clear-sky bias:

e_clear = TCWV_clear – TCWV_all (5)

To determine seasonal structures, the global distributions of the absolute and relative clear-sky bias for the different seasons were determined from the monthly differences (see Fig. 4). Overall, the distributions of the clear-sky bias correspond very closely to the distributions of the sampling error, both in strength and in pattern. Moreover, the absolute and relative deviations show only slight changes between the different seasons.

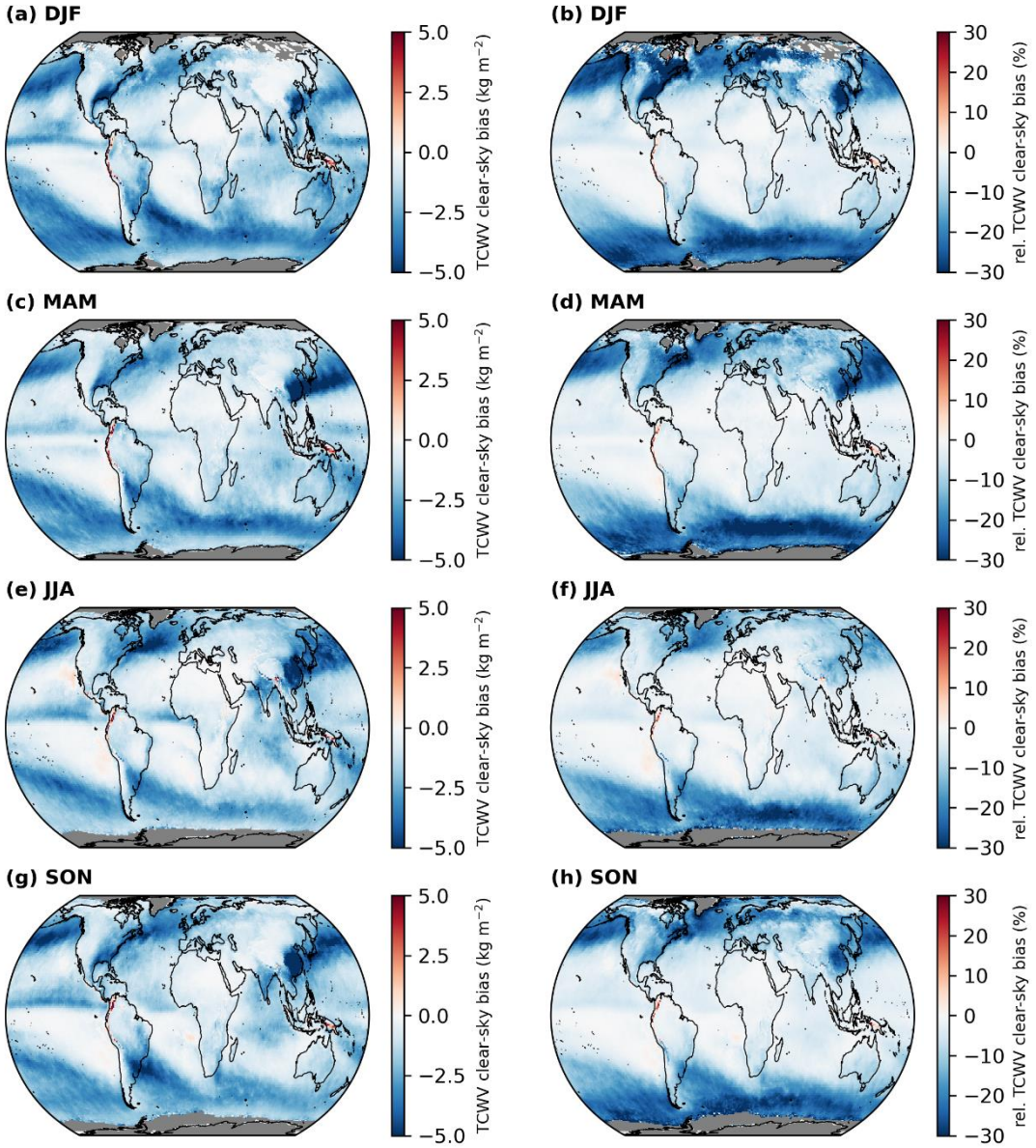

Figure 4. Global distributions of the absolute differences ("clear; left column) and relative differences ("clear=TCWVall; right column) of the monthly mean differences between clear-sky and all-sky ERA5 based on the OMI cloud information for winter (DJF; a & b), spring

(MAM, c & d), summer (JJA, e & f), and autumn (SON, g & h) for the time range January 2005 to December 2020. Grid cells for which no data is available are coloured grey.

Figures 5 and 6 summarize the sampling error and clear-sky bias distributions, respectively. For the sampling error we obtain a mean absolute deviation of -1.6 kg m-2 (median -1.4 kg m-2) and a mean relative deviation of -9.5% (-6.2%) and for the clear-sky bias we get a mean absolute deviation of -1.7 kg m-2 (median -1.3 kg m-2) and a mean relative deviation of -10.0% (-6.0%). However, the distributions of the absolute and relative deviations for the sampling error and the clear-sky bias are highly left-skewed and thus the mean value in particular is influenced by the long tails of the distributions. Nevertheless, for the clear-sky bias the obtained values agree well with the findings of Gaffen and Elliott (1993) and Sohn and Bennartz (2008). Since the effect of the clear-sky bias is already included in the sampling error and the results for both errors are very similar, it can be assumed that the spatial and temporal sampling errors play only a minor or negligible role compared to the clear-sky bias.

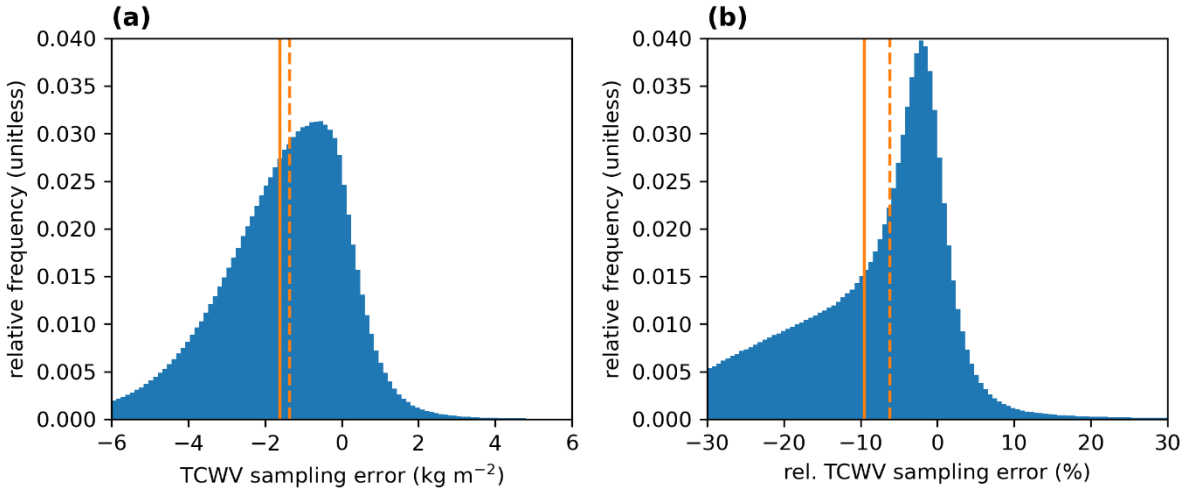

Figure 5. Distributions of the absolute differences ("sampling; Panel a) and relative differences ("sampling=TCWVtrue; Panel b) of the monthly mean differences between clear-sky and all-sky ERA5 data based on the OMI cloud information. The solid and dashed orange line indicate the mean and the median of the distributions, respectively.

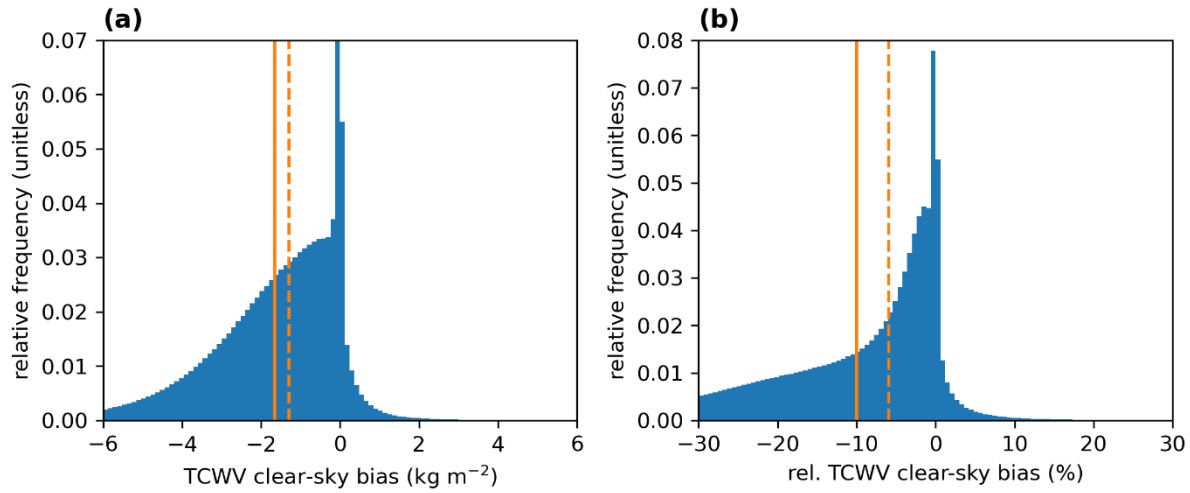

Figure 6. Distributions of the absolute differences ("clear; Panel a) and relative differences ("clear=TCWVall; Panel b) of the monthly mean differences between clear-sky and all-sky ERA5 data based on the OMI cloud information. The solid and dashed orange line indicate the mean and the median of the distributions, respectively.

In addition to the sampling error and the clear-sky bias, we also examined in Appendix C to what extent the monthly means would change if no RA-filter is applied, i.e. if all data of the complete OMI swath were available. It turns out that although deviations arise due to the RA-filter, these deviations are almost an order of magnitude smaller than those of the clear-sky bias and the global distribution of the deviations is mostly noisy. Due to this small influence of the RA-filter, we conclude that the filtered OMI TCWV data are a good representation of the actual TCWV values.

Moreover, we also investigated trends in the clear-sky bias (which has the largest impact on the sampling error) and obtained absolute trends between +-0.04 kg/m^2 per year (and -0.002kg/m^2 per year on global average), which is one order of magnitude smaller than typical TCWV trends (see e.g. Borger et al., 2022).

In conclusion, it is my feeling that the proposed data set has significant defects that are not well understood. I recommend first a more insightful analysis of the error sources, especially over land and, if possible, the elaboration of an improved version of the data set, and second, a more comprehensive discussion of the validation results in a revised version of the manuscript.

Specific comments

More should be said about the “row anomaly” which affects the OMI observations throughout almost the whole period analysed in this paper. Figure A2 shows that a large fraction of “rows” are discarded. Is it sufficient to discard these rows or could adjacent rows also be affected in some way? What is the impact of this screening on the representativeness of the final observations?

The row anomaly is a dynamic artefact and initially spread from a few isolated rows over a large area of the detector, affecting about 50% of the swath. However, it is observed that it seems to have stabilised or not changed much for a few years (see e.g. Figure 22 in

Schenkeveld et al., 2017). Based on the daily monitoring of the instrument and the rigid row-anomaly screening, we can therefore at least assume that we are filtering the very largest part of the row anomaly to the best of our knowledge, although we cannot say one hundred percent that other rows are slightly affected.

We investigated the extent to which the monthly means would change if the full swath had been taken into account and concluded that the impact is almost an order of magnitude smaller than other uncertainties (e.g. clear-sky bias). The following section is added to the appendix:

Due to the row anomaly filter, approximately 50% of the complete satellite swath of OMI is not considered in the TCWV data set. This raises the question of how much the monthly mean values would differ if the data of the complete swath were available. To investigate this, we follow the same scheme as in Sect. 3 and use the same ERA5 data as a reference. We select the ERA5 data to match the OMI overpass, once applying the row-anomaly filter and once not. However, in both cases the clear-sky filter based on the OMI cloud information is applied (effective cloud fraction < 20%).

Compared to the clear-sky bias, the deviations are much weaker and no particular spatial patterns are discernible in the global distributions except in the deep Pacific tropics and parts of Southeast Asia (see Fig. C1). Furthermore, the histograms for the absolute and relative deviations in Fig. C2 show a normal distribution for both cases with mean values of -0.30 kg m-2 and -2.1% (and for the median -0.23 kg m-2 and -1.1%). Considering the much larger uncertainties of the OMI TCWV retrievals of typically 20% and more and that the clear-sky bias is almost one order of magnitude larger, the obtained deviations are negligible and thus the monthly means from the RA-filtered data are a good representation compared to the monthly means from the data for a full swath, even though only half of the satellite data is actually used.

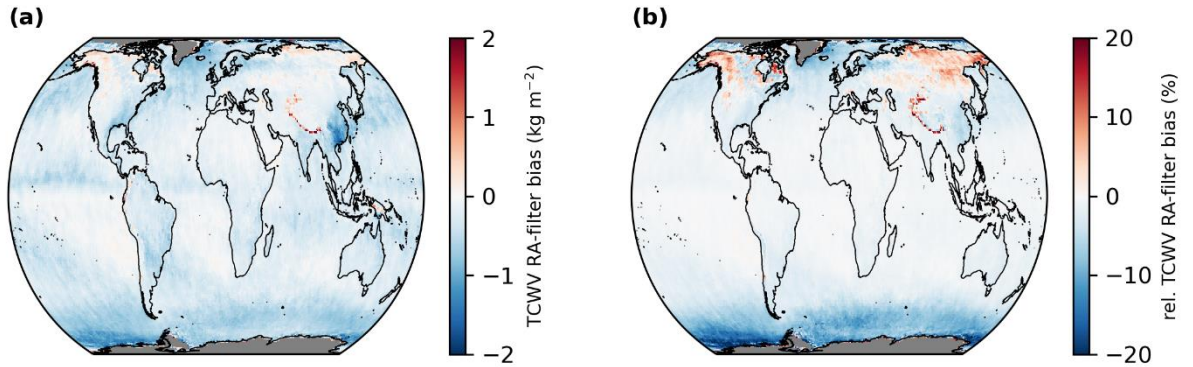

Figure C1. Global distributions of the monthly mean differences between row-anomaly (RA) filtered and full swath ERA5 based on the OMI cloud information for the time range January 2005 to December 2020. Panel (a) depicts absolute differences (i.e. RA-filtered minus full swath) and Panel (b) relative differences (i.e. (RA-filtered minus full swath) / full swath). Grid cells for which no data is available are coloured grey.

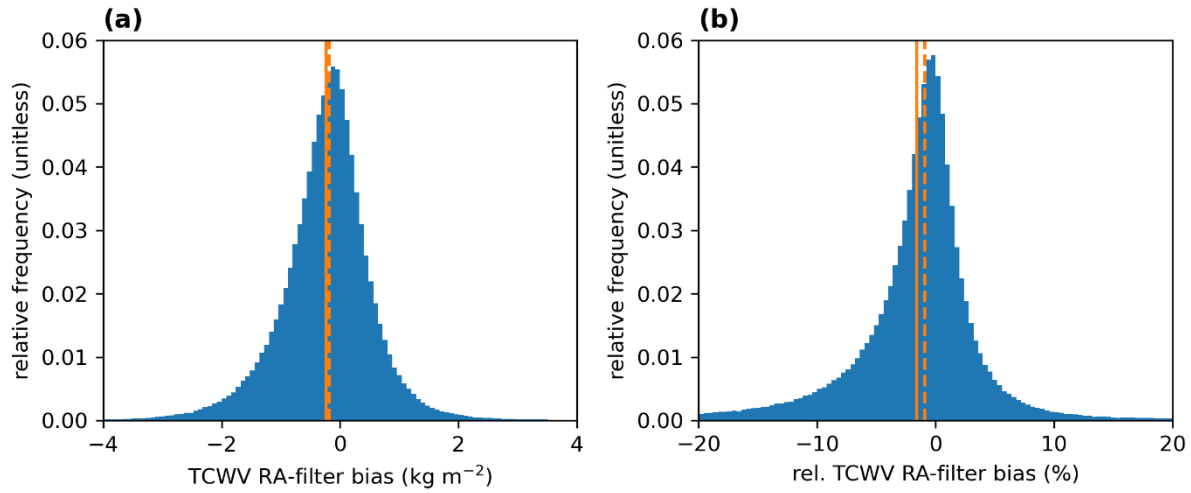

Figure C2. Distributions of the absolute differences (RA-filtered minus full swath; Panel a) and relative differences ((RA-filtered minus full swath) / full swath; Panel b) of the monthly mean differences between RA-filtered and full swath ERA5 data based on the OMI cloud information. The solid and dashed orange line indicate the mean and the median of the distributions, respectively.

So, although about 50% of the orbit is missing, this still covers a swath of about 1300km and is thus still larger than the swaths of GOME-1, SCIAMACHY or GOME-2A (all around 960km) or in the order of magnitude of SSMI (about 1394km). Thus, OMI still achieves a complete coverage of the Earth about every 2-3 days, which should provide enough observational data for a good representativeness in the case of a monthly mean (see also the good agreement with the reference data).
We added this information to the revised manuscript:
So while about 50% of the orbit is missing because of the RA-filter, the remaining data still cover an "effective" swath of about 1300 km and is thus still larger than the swaths of GOME-1, SCIAMACHY, or GOME-2A (all about 1300 km) or of the order of SSM/I (about 1394 km). Thus, OMI still achieves complete coverage of the Earth about every 2-3 days, which should provide enough observational data for good representativeness in case of a monthly mean (see also Appendix C and the good agreement to the reference data in Sect. 4).

Why are two regression methods (OLS and ODR) used? In principle, a single statistic is sufficient, unless the difference of results from the two are discussed, but this is not done in this manuscript. I suggest either to choose one or to better justify the choice of two and analyse the obtained differences.
We decided to use only the ODR, but also to show the results of the PWLF regression in the scatterplots instead.

L77: replace "I and I0" by "I0 and I"
We replaced the terms accordingly.

L129: define also Delta_SCD
We have added that Delta_SCD is the offset between Earthshine and normal SCD.

L144: indicate which fraction of raw data is remaining
If we only take the data that is already filtered according to the row anomaly as a basis, approx. 30% remains. If we take all the data of an orbit as a basis, approx. 12% remain.

However, this also includes pixels above the polar regions for which a spectral analysis is not possible or does not make sense due to the high noise.
We added the following text:
In total, this leaves about 30% of data from an RA-filtered orbit and about 12% of data from a complete orbit.

L154: "ESA Water Vapour CCI climate data record CDR-2" needs a reference
At the moment, no reference for the data set is available yet.

L154: "For the correlation analysis" is misleading or incorrect if referring to regression analysis. Please reword (e.g. For the intercomparison...)
We have changed the phrase accordingly.

L155: add a reference for the ODR method
We have added Cantrell (2008) as a reference.

L155-156: "In the case of the ODR it is necessary to use reasonable ratios of the relative errors of the compared data sets instead of using absolute errors in order to obtain meaningful results". This statement needs to be justified by an adequate explanation or reference.
Based on the descriptions of Cantrell (2008), one sees in equation (5) in his paper that the slope depends on a parameter W_i, which relates the uncertainties w_x and w_y of x and y to each other (see formula below).

$$
\begin{aligned}
& b = \overline{y} - m\ \overline{x}\ \ m = \frac{\sum W_i \beta_i V_i}{\sum W_i \beta_i U_i} \\
& \overline{x} = \sum W_i x_i \Big/ \sum W_i\ \ \overline{y} = \sum W_i y_i \Big/ \sum W_i \\
& U_i = x_i - \overline{x}\ \ V_i = y_i - \overline{y}\ \ W_i = \frac{w_{xi} w_{yi}}{w_{xi} + m^2 w_{yi} - 2 m r_i \alpha_i} \\
& \beta_i = W_i \left[\frac{U_i}{w_{yi}} + \frac{m V_i}{w_{xi}} - (m U_i + V_i) \frac{r_i}{\alpha_i} \right] \quad \alpha_i = \sqrt{w_{xi} w_{yi}}
\end{aligned}
\qquad (5)
$$

In the case that the error in y is significantly larger than in x, the ODR approaches ordinary linear regression.

Cantrell, C. A.: Technical Note: Review of methods for linear least-squares fitting of data and application to atmospheric chemistry problems, Atmos. Chem. Phys., 8, 5477–5487, https://doi.org/10.5194/acp-8-5477-2008, 2008.

L156-159: these sentences sound in contradiction with the previous statement. Moreover, the sensitivity of the regression results to the relative errors should be discussed in more detail (e.g. in an Appendix) and the choice of 5%, 10%, and 20% for the three dataset (which appear quite arbitrary) should be clearly motivated/discussed.
To motivate our choice, we have added the following text to the revised version:
Mears et al. (2015) found that the uncertainty of daily microwave TCWV observations for TCWV=10 kg m-2 was around 1 kg m-2 and for TCWV = 60 kg m-2 around 2-4 kg m-2. Hence, we assume that the uncertainty of the RSS data set is 5% or at least 1 kgm−2. For

ERA5 and ESA CDR-2 we can assume similar uncertainties over ocean, since the TCWV values there are also mainly based on microwave observations. Unfortunately, no uncertainties are provided for TCWV over land. Thus, for the sake of simplicity, we assume that the relative errors of the reference data sets over land are twice as high as over ocean, i.e. 10% or at least 2 kg m-2. For the OMI TCWV data set we assume an uncertainty of 20% (Borger et al., 2020), but at least 2kg m-2. We also tested other error assumptions and it turned out that the exact choice of errors is negligible for the regression results as long as the ratio of uncertainties remains similar.

L169-171: "In general the deviations are quite low with values between +/- 2.5 kg/m2" be more specific in quantifying the differences here, e.g. indicate which fraction of data lie in the range of +/-2.5 kg/m2, or use quantiles or other statistics (mean, standard deviation, etc.). Note also that the correlation coefficient is not much relevant when the seasonal variations are included.

We added the information of the mean bias together with the standard deviation for the comparison to every data set and also provide this information for the tropics (-20°N – 20°N) and for the extratropics.

With regard to the correlation coefficient, we cannot fully agree, as it includes spatial variation in addition to temporal variation: namely, if we reverse the latitudes, we only obtain a correlation of R=0.63 for RSS and R=0.45 for ERA5 over land.

L173-178: Be more quantitative again, here in the comments on Fig. 4. I would also suggest to include the coastlines of Africa and Indonesia in the list of regions with significant positive deviations.

As mentioned above, we now provide the mean bias and the standard deviation. Moreover, we rephrased the sentence:

Consistent with the findings from Fig. 7 highest positive deviations can be found in the tropical Pacific ocean and near the coastlines of South America, Africa, and Indonesia whereas […]

L176: Be more specific on the impact of the "cold tongue" and "too low albedo" on the observed deviations.

The area of the "cold tongue" is often affected by low maritime clouds (cloud top height at approx. 1km). Since the highest water vapour concentration are found in the lower troposphere or boundary layer, deviations in the AMF of the order of 10% can occur even with slightly deviating cloud heights of a few 100m.

In the area of Central America and the west coast of Africa, the albedo is influenced by the absorption by phytoplankton (Kleipool et al., 2008), which may not have been optimally corrected during the creation of the LER or ensures that already low albedo values can lead to further small deviations, which are then again large in relative terms (e.g. with albedo values of 0.05 to 0.04).

We rephrased the text as follows:

In the case of the tropical Pacific ocean the distribution of the systematic positive deviations matches quite well regions of cold water or of the so called "cold tongue" which is frequently affected by low clouds. Since the highest water vapour concentrations occur in the lower troposphere, small deviations of a few 100m in cloud height can have relatively large effects on the AMF. In the case of Central America or Atlantic ocean, a too low albedo due to additional absorption by phytoplankton (Kleipool et al., 2008) could explain the systematic positive deviations.

L182: “the slight overestimation of 3-5%”: it is not clear what these numbers represent exactly. Is it a mean difference (bias)? Is it computed over all data or only a fraction? (Note that a slope of 1.03 does not mean that all the values are 3% higher, this depends also on the intercept value).
Many thanks for this hint! Indeed, we have not expressed our approach clearly enough. By 3-5% overestimation, we are referring to the slope of the fit line. Regarding the y-axis intercept, we will explicitly mention it if it is larger than the minimum assumed uncertainty (1kg over ocean, 2kg over land). For the ocean comparisons, the offsets are less than +-0.25kg/m^2, so they are negligible and thus the slope is sufficient as the sole indicator of over- or underestimation. For the comparisons for the data over land, however, they are systematically higher than the minimum uncertainty, so we have revised the text of the respective comparisons:
For data over land, the picture is different: although the ODR gives similar results for the slope as for data over ocean, the distribution in the 2D histogram (Fig. 9c) shows particularly strong positive deviations of approximately +10 kg m−2 at high TCWV values and an overall systematic offset of around +1.43 kg m−2.Within the PWLF analysis we find a good agreement to the reference data for TCWV values up to about 25 kg m−2 (which represents approximately 74% of all data points) with slopes of around 0.96. However, for higher TCWV values we find distinctive positive overestimations of up to 24%. Nevertheless, even for low TCWV values a systematic offset of approximately +2.52 kg m−2 is obtained.
[…]
Similar to the intercomparison of ERA5, the intercomparison over land (Fig. 11c) shows roughly similar ODR fit results as over ocean, but here we also find striking positive deviations for high TCWV values and an overall positive offset of 2.41 kg m−2. Again, when applying a piecewise linear regression analysis we obtain good agreement with slopes of around 0.95 for TCWV values to about 25 kgm−2 but still a distinctive positive offset of 3.73 kg m−2 for low TCWV values and distinctive overestimations of up to 33% for higher TCWV values, which is even higher than for the comparison to ERA5.

L194: how is the change-point at 26 kg/m2 selected in the piecewise linear regression?
The change point is automatically determined by a non-linear least-squares fit.

L210: satellite measurements in the thermal infrared are NOT available/reliable in cloudy conditions.
We have reworded the sentence as follows:
[…] satellite measurements (or none at all in the thermal infrared) […]

L209-215: I’m not convinced that the ERA5 uncertainty over tropical land areas contributes much to the huge bias observed in the differences (above 10 kg/m2). This idea should be further documented or discarded (also in the Conclusion).
The regions in question are highly affected by quasi-permanent cloud cover, so observations are systematically missing and there may be a clear-sky bias, which can be in the order of a few kg/m^2 (see also Sect. 3 in the revised manuscript). And even if radiances are assimilated into cloudy-sky scenarios, their uncertainty is still large, as the radiative transfer of cloudy pixels is highly complex (e.g. Li et al., 2016). Especially even in the ESA WV_cci CDR these regions are flagged, although MODIS should have enough observations available for good statistics. We conclude that the large deviations in the tropics cannot, of course, be completely attributed to the uncertainties in ERA5, but they are not so small as to be negligible either.

Li, J., Wang, P., Han, H. et al. On the assimilation of satellite sounder data in cloudy skies in numerical weather prediction models. J Meteorol Res 30, 169–182 (2016). https://doi.org/10.1007/s13351-016-5114-2

L227: is there any update on the publication of the ESA CDR-2 data set?
To the best of our knowledge, no publication is available at the moment.

L225-254: Similar comments as for ERA5 apply here to the CDR-2 comparison (lack of statistics, etc.).
See comment above about added statistics.

L261: More details are needed on the linear regression method and significance tests.
For the analysis, we use an ordinary least-squares fit, with the significance test or p-value based on a two-sided Students t-test (see also https://docs.scipy.org/doc/scipy/reference/generated/scipy.stats.linregress.html). We added this information in the revised manuscript as follows:
[…] and then calculate temporal trends of these deviations using linear ordinary linear least-squares regression following the approach of Danielczok and Schröder (2017) and Beirle et al. (2018) and assess the significance of the results based on a two-sided Student's t-test.

L274: The stability requirement for water vapour climate data is rather at the level of 0.3 %/decade (GCOS – 112, April 2007).
See comment above in the General Comments section.

Figure 3: the fit results would be more understandable if given as an equation: y = 1.03 x + 0.18 rather than just two numbers.
We have changed the legends in the figures accordingly.

Figure 3: indicate that the OMI results here are over ocean (it is only obvious if one knows that SSM/I data over only over the oceans).
We added in the Figure caption that the results correspond to data over ocean.

Figure 4: add the piecewise linear regression lines (mentioned L194) on the plot.
We have added information of the PWLF regression results in all relevant figures.

Figure 9: the red dashed lines are not visible in the plots.
We revised Figure 9 and removed the dashed red lines.

We would like to thank the referee for reviewing our manuscript and for the many useful comments and suggestions. Below we reply to the issues raised by the referee, where
blue repeats the reviewer's comments,
black is used for our reply,
and green italics is used for modified text and new text added to the manuscript.

A 16-year global climate data record of total column water vapour generated from OMI observations in the visible blue spectral range
Christian Borger, Steffen Beirle, and Thomas Wagner

1. General Comments
This paper assesses a long term record (2005-2020) of monthly mean total column water vapour (TCWV) from the Ozone Monitoring Instrument (OMI) on board NASAs Aura platform. The authors describe adaptations to an existing algorithm used for ESAs TROPOMI instrument, which is seen as a successor to OMI. This includes the rational for the how and why they switch to using earth shine spectra as the reference in the DOAS retrieval setup. This study goes on to present results from an inter-comparison of TCWV against two addition remote sensing products from RSS and ESA and ERA5 reanalysis.

While this study does discuss issues to do with sampling, I feel this could be expanded especially relating to the clear-sky bias. Work on this has been done within the ESA water vapour CCI project, results from which are relevant to this study and would enhance the discussion around the OMI product performance.
Many thanks for this important comment! We agree with the reviewer and have decided to estimate the clear-sky bias within our data set. Moreover, following the suggestions from Reviewer #1, we also estimate sampling errors. As such, we have added the following text to the revised version:
Although satellite observations enable the analysis of trace gas concentrations on global scale, a fundamental problem is that typically a satellite measurement is only taken once a day for one location. Furthermore, satellite measurements are usually only available under cloud-free conditions, especially in the visible or infrared spectral range and thus no continuous time series is guaranteed. Consequently, they cannot provide a complete picture of geophysical variability, which leads to sampling errors in the calculation of averaged values (e.g. monthly means).
Moreover, the question arises to what extent the limitation to cloud-free pixels influences the monthly averages determined from the OMI satellite measurements, i.e. whether in the OMI TCWV data set a so-called "clear-sky bias" exists. Gaffen and Elliott (1993) investigated this bias using radiosonde ascents and found that the TCWV is about 0-15% lower under cloud-free conditions than under cloudy conditions. Similarly, Sohn and Bennartz (2008) found a clear-sky bias between MERIS and AMSR-E of about 10%.
To estimate the sampling errors, we follow the methods of Xue et al. (2019) and Gleisner et al. (2020): we choose hourly-resolved ERA5 data with a spatial resolution of 0.25°x 0.25° as reference data and collocate the ERA5 data with OMI overpass times. These data are then resampled to the 1°x1° resolution of the OMI TCWV data set and the monthly averages are calculated (TCWV_sampled). We then take the complete, original ERA5 data, resample it to the same spatial resolution and calculate monthly means from this data as well (TCWV_true). The difference between the two data sets then represents the sampling error:

$$e_{sampling} = TCWV_{sampled} - TCWV_{true} \quad (4)$$

With this definition, the sampling error summarises the uncertainties due to gaps in the swath, temporal differences or missing data (e.g. due to clouds) (Xue et al., 2019).
Figure 3 shows the annual mean absolute and relative sampling errors for the year 2006. Overall, it can be seen that most deviations are negative, i.e. the actual TCWV is underestimated. Regarding the absolute deviations, the strongest deviations can be seen in the area of storm-tracks in the mid-latitudes (e.g. North Atlantic) and the polar regions with values around -5 kg m-2. The smallest deviations are found in the quasi-permanent cloud-free regions in the subtropics. As expected, the relative differences increase from the equator towards the poles due to the decreasing TCWV values and reach values stronger than -30%.

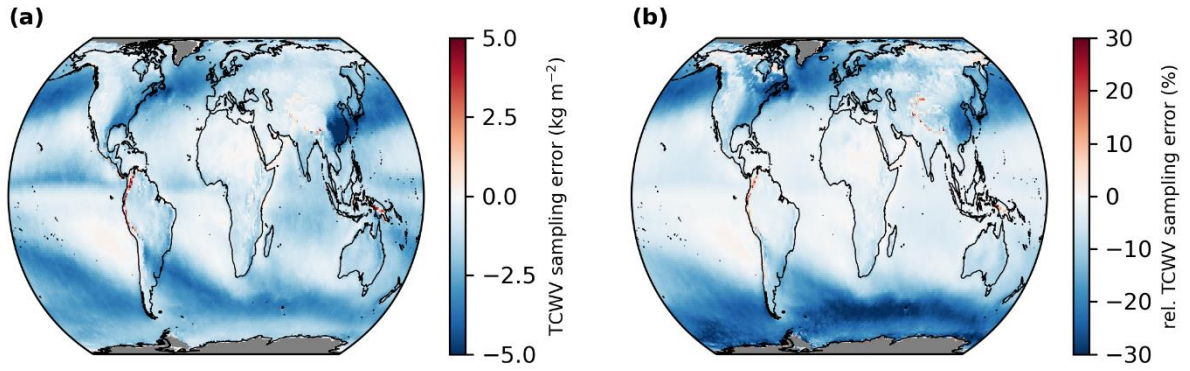

Figure 3. Global distributions of the mean sampling errors derived from monthly mean sampling differences for the time range January 2005 to December 2020. Panel (a) depicts absolute sampling error (i.e. "sampling) and Panel (b) relative sampling error (i.e. "sampling=TCWVtrue). Grid cells for which no data is available are coloured grey.

To investigate to what extent these deviations are related to the clear-sky bias, we proceed similarly to the calculation of the sampling error: we collocate the ERA5 data to the OMI overpass time and once apply a cloud filter (effective cloud fraction < 20%) and once not. Then we resample both data sets to 1°x 1° and calculate monthly means. The difference of both data sets then represents the clear-sky bias:

e_clear = TCWV_clear – TCWV_all (5)

To determine seasonal structures, the global distributions of the absolute and relative clear-sky bias for the different seasons were determined from the monthly differences (see Fig. 4). Overall, the distributions of the clear-sky bias correspond very closely to the distributions of the sampling error, both in strength and in pattern. Moreover, the absolute and relative deviations show only slight changes between the different seasons.

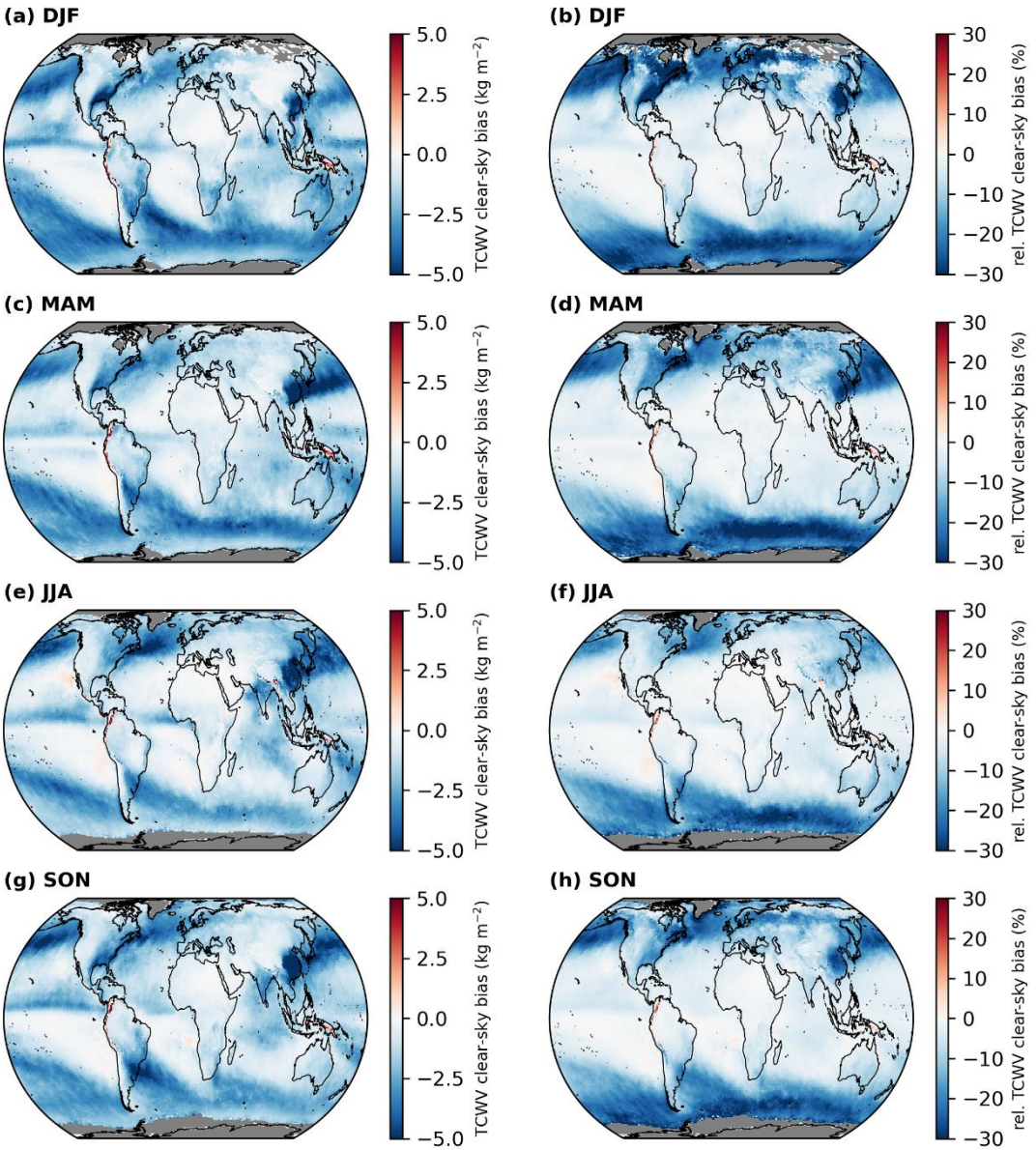

Figure 4. Global distributions of the absolute differences ("clear; left column) and relative differences ("clear=TCWVall; right column) of the monthly mean differences between clear-sky and all-sky ERA5 based on the OMI cloud information for winter (DJF; a & b), spring (MAM, c & d), summer (JJA, e & f), and autumn (SON, g & h) for the time range January 2005 to December 2020. Grid cells for which no data is available are coloured grey.

Figures 5 and 6 summarize the sampling error and clear-sky bias distributions, respectively. For the sampling error we obtain a mean absolute deviation of -1.6 kg m-2 (median -1.4 kg m-2) and a mean relative deviation of -9.5% (-6.2%) and for the clear-sky bias we get a mean absolute deviation of -1.7 kg m-2 (median -1.3 kg m-2) and a mean relative deviation of -10.0% (-6.0%). However, the distributions of the absolute and relative deviations for the sampling error and the clear-sky bias are highly left-skewed and thus the mean value in particular is influenced by the long tails of the distributions. Nevertheless, for the clear-sky bias the obtained values agree well with the findings of Gaffen and Elliott (1993) and Sohn and Bennartz (2008). Since the effect of the clear-sky bias is already included in the sampling error and the results for both errors are very similar, it can be assumed that the spatial and

temporal sampling errors play only a minor or negligible role compared to the clear-sky bias.

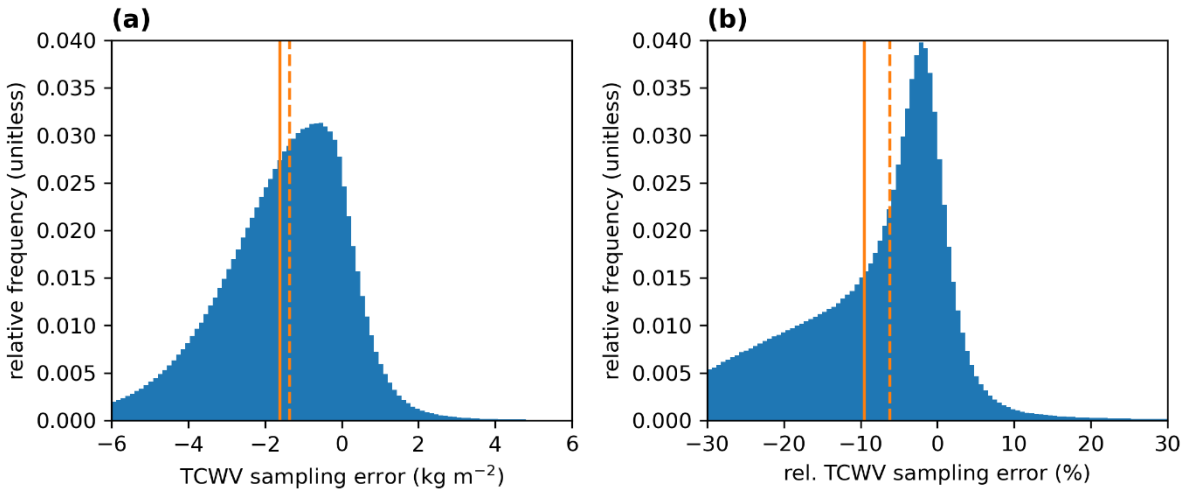

Figure 5. Distributions of the absolute differences ("sampling; Panel a) and relative differences ("sampling=TCWVtrue; Panel b) of the monthly mean differences between clear-sky and all-sky ERA5 data based on the OMI cloud information. The solid and dashed orange line indicate the mean and the median of the distributions, respectively.

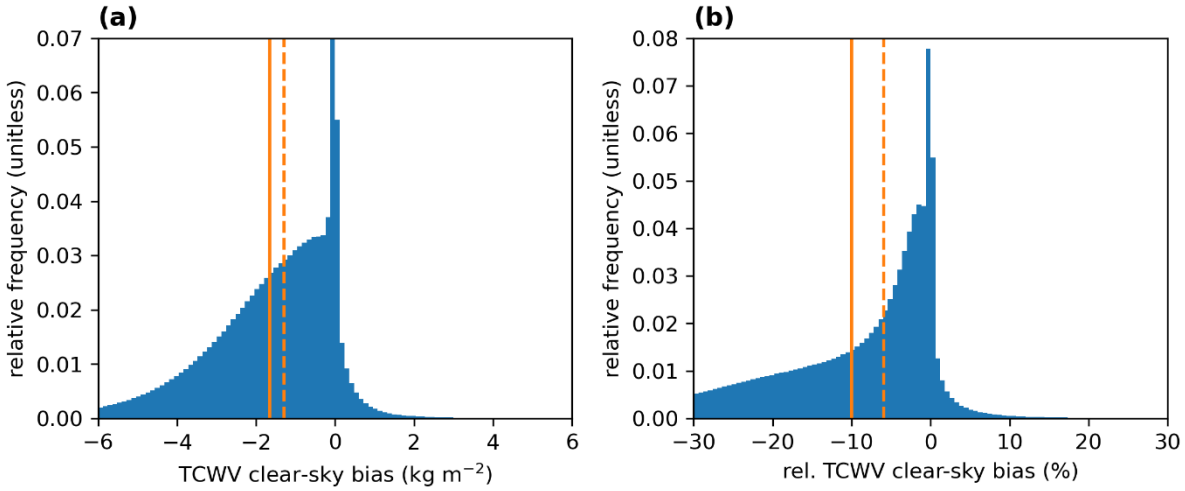

Figure 6. Distributions of the absolute differences ("clear; Panel a) and relative differences ("clear=TCWVall; Panel b) of the monthly mean differences between clear-sky and all-sky ERA5 data based on the OMI cloud information. The solid and dashed orange line indicate the mean and the median of the distributions, respectively.

In addition to the sampling error and the clear-sky bias, we also examined in Appendix C to what extent the monthly means would change if no RA-filter is applied, i.e. if all data of the complete OMI swath were available. It turns out that although deviations arise due to the RA-filter, these deviations are almost an order of magnitude smaller than those of the clear-sky bias and the global distribution of the deviations is mostly noisy. Due to this small influence of the RA-filter, we conclude that the filtered OMI TCWV data are a good representation of the actual TCWV values.

Furthermore, there is no mention regarding the quality of the datasets chosen for the inter-comparison exercise. Addition of this information at the beginning of section 3 would help inform a reader unfamiliar with these data sets to why they were used by this study.

We thank the reviewer for this suggestion and have restructured Section 3 accordingly. Moreover, we added the following text to the beginning of Sect. 3:

To evaluate the overall quality of the OMI TCWV data set, we conducted an intercomparison study for which we use the merged, 1-degree total precipitable water (TPW) data set version 7 from Remote Sensing Systems (RSS) (Mears et al., 2015; Wentz, 2015), TCWV data from the reanalysis model ERA5 (Hersbach et al., 2019, 2020), and the ESA Water_Vapour_CCI (WV_cci) climate data record CDR-2 as reference.

The RSS data set consists of merged geophysical ocean products whereby the values are retrieved from various passive satellite microwave radiometers. These microwave radiometers have been intercalibrated at the brightness temperature level and the ocean products have been produced using a consistent processing methodology for all sensors (more details in Wentz, 2015; Mears et al., 2015). The major advantages of microwave TCVW retrievals are their high precision and accuracy and that they are insensitive to clouds, so that TCWV values can also be retrieved even under cloudy-sky conditions. A disadvantage, however, is that these retrievals are (mostly) only available over the ocean surface.

Thus, we also compare the OMI TCWV data to the ESAWV_cci CDR-2. At the moment of preparation of this manuscript, the CDR-2 is a beta-version of the combined microwave and near-infrared imager based TCWV data record (COMBI). The CDR combines microwave and near-infrared imager based TCWV over the ice-free ocean as well as over land, coastal ocean and sea-ice, respectively. The data record relies on microwave observations from SSM/I, SSMIS, AMSR-E and TMI, partly based on a fundamental climate data record (Fennig et al., 2020) and on near-infrared observations from MERIS, MODIS-Terra and OLCI (Danne et al., 2022).

Within comparisons between different satellite data sets a major drawback is the influence of sampling errors due to different observation times, pixel footprint sizes or orbit patterns. To minimise this source of error, data from reanalysis models are useful. ERA5 is the fifth generation ECMWF reanalysis (Hersbach et al., 2020) and combines model data with in situ and remote sensing observations from various different measurement platforms. For our purpose, we use the "monthly averaged reanalysis by hour of day" from the Copernicus Climate Data Store on a 1°x 1° grid. To account for OMI's observation time (around 13:30 LT), we first calculate the local time for each longitude in the ERA5 data set, then select the TCWV data for the time period between 13:00-14:00 LT and finally merge the selected data.

[…]

Finally, what is not clear is to whether this new data record from OMI is meant to complimentary to the existing TROPOMI data set? By this, I mean could the records be used sequentially to bring the time series out the end of the TROPOMI mission? I this is the case, how does the performance of these two record compare?

Indeed, in the future we plan to merge the TCWV datasets of OMI and TROPOMI or to continue the OMI dataset using TROPOMI data. For the time being, however, we are refraining from doing so:

- the TROPOMI cloud algorithms are not yet fully developed and there are currently repeated jumps in the TROPOMI TCWV dataset (see for example Küchler et al., 2021).

- the OMI radiances have been processed with the TROPOMI processor since 2022 and will also be reprocessed with it after the end of the mission. This should lead to an improvement of the irradiance and radiance spectra, so that it may be possible to switch from an Earthshine fit to a solar irradiance fit.
- OMI will soon run out of fuel and thus the mission will end soon (2023 or 2024). By then, there should also be enough overlap between OMI and TROPOMI.

Overall, I find that this study is of scientific value and recommend it for publication, after all the issues that I have highlighted are addressed.

2. Specific Comments

- Section 3: I think the term validation here is incorrect as you are performing inter-comparison of the OMI performance against other gridded products at monthly time scales. For this to be a validation study you would need to perform this on the level 2 swath data against ground truth sites. Alternatively, accurate (fiducial) characterisation of these reference products on monthly time scales would need to be done, and this would be a major undertaking in itself.

We agree that the term "validation" is not adequate and will instead refer to an "intercomparison study".

- Lines 157-158: What is the assumption you base the relative error estimates on? From the literature, or results not included in this paper? Are you actually describing uncertainties or do you mean errors? Further elaboration here would make this clearer to the reader.

For SSMI, we followed the results of Mears et al. (2015), who found that the uncertainty for TCWV = 10mm was around 1mm and for TCWV = 60mm around 2-4mm. Thus, we have revised the uncertainties again and specify that the uncertainty is 5% or at least 1mm.
For ERA5 and ESA CDR we can assume similar uncertainties over ocean, since the TCWV values there are also mainly based on microwave observations. For the ESA CDR, "average retrieval uncertainties" are given, but these are unrealistically low over land (<0.1kg/m^2). Therefore, we decided to make a compromise and, for simplicity's sake, set the uncertainty about twice as high as the uncertainty over ocean.
We added the following text to the revised manuscript:
Mears et al. (2015) found that the uncertainty daily microwave TCWV observations for TCWV=10 kg m-2 was around 1 kg m-2 and for TCWV = 60 kg m-2 around 2-4 kg m-2. Hence, we assume that the uncertainty of the RSS data set is 5% or at least 1 kgm−2. For ERA5 and ESA CDR-2 we can assume similar uncertainties over ocean, since the TCWV values there are also mainly based on microwave observations. Unfortunately, no uncertainties are provided for TCWV over land. Thus, for the sake of simplicity, we assume that the relative errors of the reference data sets over land are twice as high as over ocean, i.e. 10% or at least 2 kg m-2. For the OMI TCWV data set we assume an uncertainty of 20% (Borger et al., 2020). We also tested other variants of error assumptions and it turned out that the exact choice of errors is negligible for the regression results as long as the ratio of uncertainties remains similar.

- Section 3.2: For the ERA5 did you take the hourly data and interpolate to the local over pass time or the monthly mean data on hourly time steps? Slight rewording to clarify is needed. Additionally, did you consider using the ensemble output which would have given the spread in the reanalysis rather than assigning a relative estimate of the uncertainty?

For the ERA5 data we used the "Monthly averaged reanalysis by hour of day" from the Copernicus climate data store (CDS). Starting from the OMI overpass time (13:30LT), the local time was determined for each longitude and then the TCWV data for the period 13:00 to 14:00LT were selected and merged.
We added the following text to the revised manuscript:
For our purpose, we use the "monthly averaged reanalysis by hour of day" from the Copernicus Climate Data Store on a 1° x 1° grid. To account for OMI's observation time (around 13:30 LT), we first calculate the local time for each longitude in the ERA5 data set, then select the TCWV data for the time period between 13:00-14:00 LT and finally merge the selected data.

Regarding the use of ERA5 ensemble data, we have to admit that we are not experts in this field and therefore cannot completely understand how the different ensemble members come about. Nevertheless, we have taken a look at the ensemble data and calculated the ensemble spread and the relative spread as follows:
Spread = max(ensemble) - min(ensemble)
Relative spread = Spread / mean(ensemble)

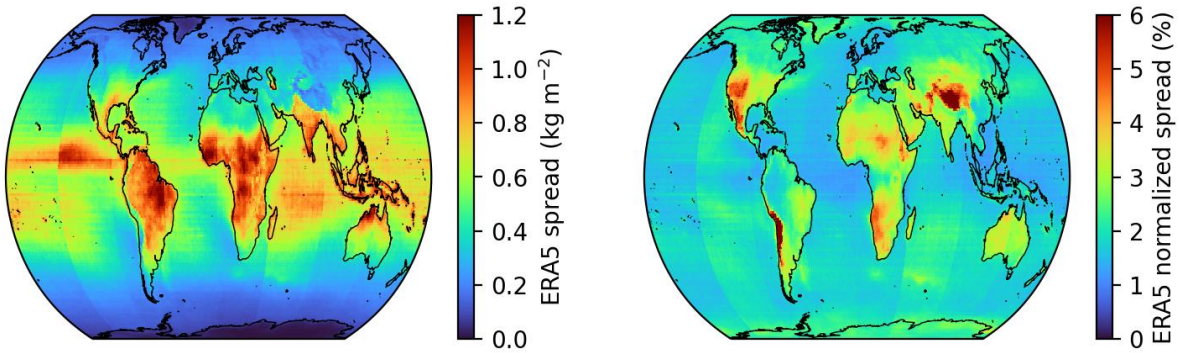

Fig.RC1: Spread (left) and relative spread (right panel) of ERA5 TCWV ensemble data at around 13:30LT derived from 3-hourly resolved monthly mean by hour of day TCWV data for the time range January 2005 to December 2020. The local time was determined by longitude. Then the data was selected for a time between 12:00 and 15:00LT and finally merged.

In our opinion, however, these spreads underestimate the actual uncertainty of ERA5: Over the ocean, the uncertainties are smaller than in the SSM/I (see comment above), although similar input data should be used. And over land they are in some places only slightly larger than over the ocean, which is not entirely understandable, since much less observational data is available than over the ocean, or over land the (satellite) measurements typically have a larger uncertainty.
Therefore, we believe that our assumption for the uncertainty, is a good estimate of the uncertainties in ERA5.

- Figure 7/B3: The comparison to ESA CCI over land – did you also apply stricter cloud filtering to the OMI data as well as the common mask? The improvement in representativeness can be seen in figure B3 but there could still be additional cloud in the OMI data which is biasing the data. The common mask from the ESA data will be for 10:00 hrs LST, while with OMI overpasses at 13:30 hrs LST which will have an impact in convective areas. Finally, is there an improvement in the Hovmöller time series when the common mas is applied?

Following the suggestion of the reviewer, we have also applied a more stringent cloud filter (CF<5% instead of CF<20%) and have carried out the comparisons with it. For the sake of simplicity, we only show the comparisons with ERA5.
When looking at the difference maps for each season, a clear reduction of the systematic overestimation in the tropics or in the Amazon region can be seen on average, but we now also see clear underestimation in areas with frequent cloud cover (e.g. India or Southeast Asia). This indicates that such a stringent filter leads to a strong clear-sky bias. Furthermore, the filter leads to many gaps in the TCWV data set, so that it would no longer be optimal for time series studies.
Therefore, we think that the current configuration with CF<20% is a good compromise between spatiotemporal coverage and quality.

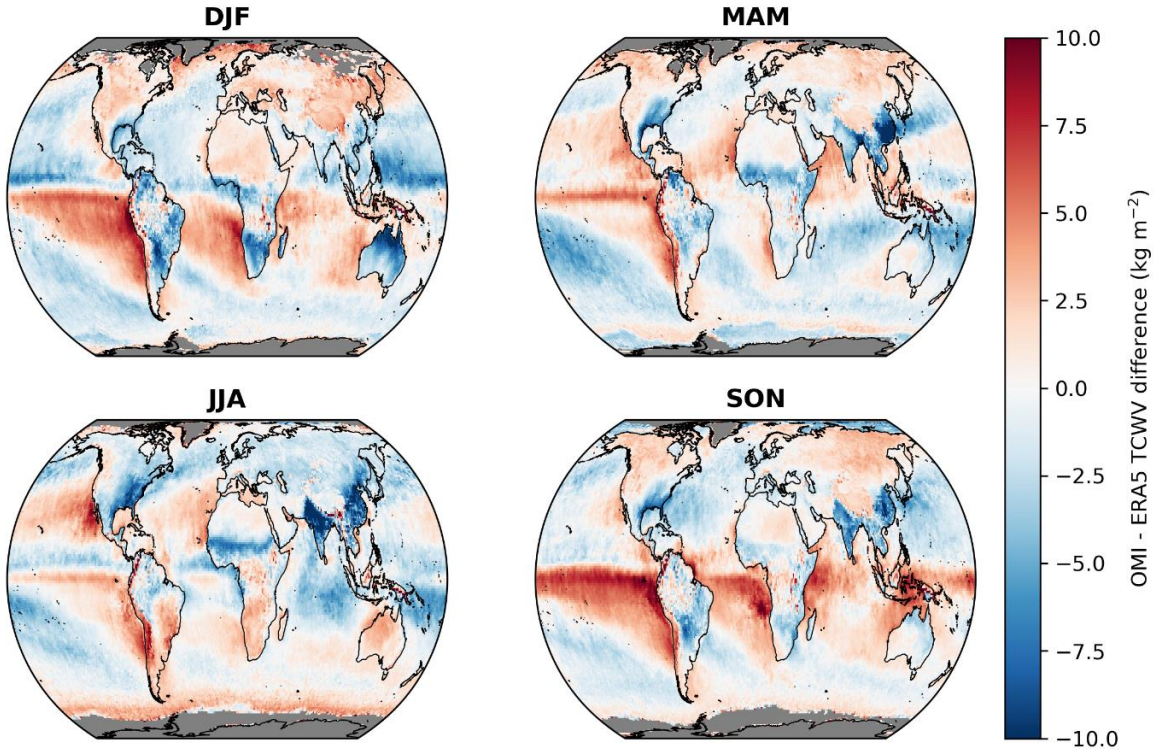

Fig. RC2: Global distributions of the absolute differences between the OMI TCWV data with a stricter cloud filter (eCF < 5%) and ERA5 for winter (DJF), spring (MAM), summer (JJA), and autumn (SON). Grid cells for which no data is available are coloured grey.

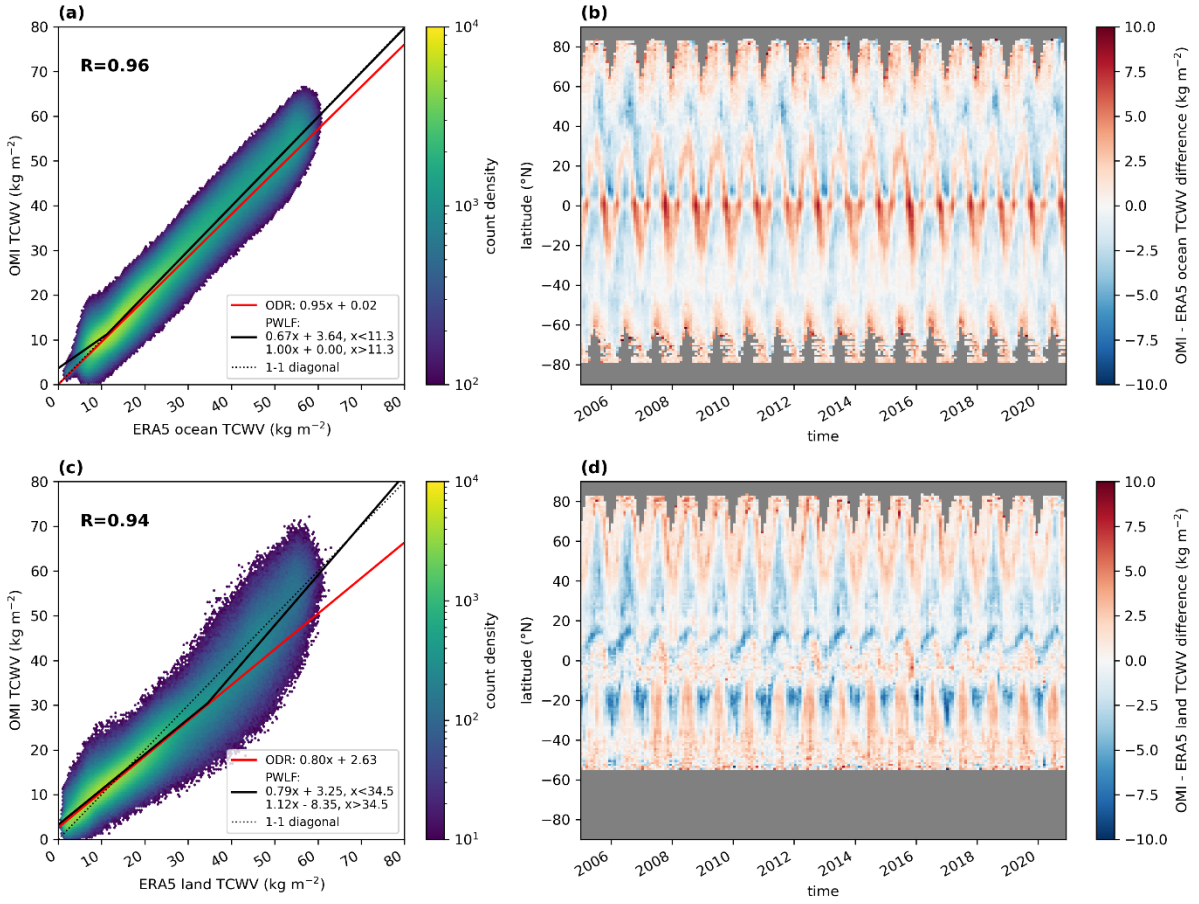

Fig. RC3: Intercomparison between monthly mean TCWV from OMI (with the stricter cloud filter) and ERA5 for data over ocean (top row) and land (bottom row). Panel (a) and (c) illustrate a 2D histogram in which the colour indicates the count density; the red solid line represents the results of the orthogonal distance regression (ODR) and the solid black line the results of the piecewise linear regression (PWLF). The results of the respective fits are given in the bottom right box and the correlation coefficient in the top left corner. The dashed black line indicates the 1-to-1 diagonal. Panels (b) and (d) depict the TCWV difference of OMI minus ERA5 within the latitude-time space; reddish colours indicate an overestimation, blueish colours an underestimation of the OMI TCWV data set.

3. Technical Comments

- Line 38: the reference Susskind et al. 2003 is for joint microwave and infrared retrievals from AIRS. Therefore, is not an explicit reference for IR water vapour retrievals. There is also an extra ‘)’ on line 39 after the reference, did you mean to have the 2003 in-cased in parenthesises?

Thank you for the clarification regarding the Susskind et al. reference! We have added the references of Schlüssel et al. (2005) and Schneider and Hase (2011) as examples of TIR retrievals.

- Line 39: both your references here are for near infrared retrievals from MERIS, missing a shortwave infrared reference e.g. SCIAMACHY (2.3 µm), GOSAT (1.6 +2.1 µm), or TROPOMI (2.3 µm).

We have added the references of Schrijver et al. (2009), Dupuy et al. (2014) and Schneider et al. (2020) as examples of SWIR retrievals.

A 16-year global climate data record of total column water vapour generated from OMI observations in the visible blue spectral range

Christian Borger, Steffen Beirle, and Thomas Wagner

Satellite Remote Sensing Group, Max Planck Institute for Chemistry, Mainz, Germany

Correspondence: Christian Borger (christian.borger@mpic.de) and Thomas Wagner (thomas.wagner@mpic.de)

Abstract. We present a long-term data set of $1° \times 1°$ monthly mean total column water vapour (TCWV) based on global measurements of the Ozone Monitoring Instrument (OMI) covering the time range from January 2005 to December 2020.

In comparison to the retrieval algorithm of Borger et al. (2020) several modifications and filters have been applied accounting for instrumental issues (such as OMI's "row-anomaly") or the inferior quality of solar reference spectra. For instance, to overcome the problems of low quality reference spectra, the daily solar irradiance spectrum is replaced by an annually varying mean Earthshine radiance obtained in December over Antarctica. For the TCWV data set only measurements are taken into account for which the effective cloud fraction < 20%, the AMF > 0.1, the ground pixel is snow- and ice-free, and the OMI row is not affected by the "row-anomaly" over the complete time range of the data set. The individual TCWV measurements are then gridded to a regular $1° \times 1°$ lattice, from which the monthly means are calculated.

The investigation of sampling errors in the OMI TCWV dataset shows that these are dominated by the clear-sky bias and cause on average deviations of around -10%, which is consistent with the findings from previous studies. However, the spatiotemporal sampling errors and those due to the row anomaly filter are negligible.

In a comprehensive validation intercomparison study we demonstrate that the OMI TCWV data set is in good agreement to reference data sets of ERA5, RSS SSM/I, and ESA CCI Water Vapour Water Vapour CCI CDR-2: over ocean ordinary least squares (OLS) as well as orthogonal distance regressions orthogonal distance (ODR) and piece-wise linear regressions (PWLF) indicate slopes close to unity with very small offsets and high correlation coefficients of around 0.98. However, over land, distinctive positive deviations are obtained especially within the tropicswith relative deviations of approximately +10% of more than $+10\,\mathrm{kg\,m^{-2}}$ are obtained for high TCWV values. These overestimations are mainly due to extreme overestimation of high TCWV values in the tropics, likely caused by uncertainties in the retrieval input data (surface albedo, cloud information) due to frequent cloud contamination in these regions. Nevertheless, for TCWV values smaller than $25\,\mathrm{kg\,m^{-2}}$, the OMI TCWV data set shows very good agreement with the reference datasets.

Also, a temporal stability analysis proves that the OMI TCWV data set is consistent with the temporal changes of the reference data sets and shows no significant deviation trends.

Since the TCWV retrieval can be easily applied to further satellite missions, additional TCWV data sets can be created from past missions such as GOME-1 or SCIAMACHY, which under consideration of systematic differences (e.g. due to different observation times) can be combined with the OMI TCWV data set in order to create a data record that would cover a time span from 1995 to the present. Moreover, the TCWV retrieval will also work for all missions dedicated to NO_2 in future such as

Sentinel-5 on MetOp-SG.

The MPIC OMI total column water vapour (TCWV) climate data record is available at https://doi.org/10.5281/zenodo.5776718 (Borger et al., 2021).

1 Introduction

Water vapour is the most important natural greenhouse gas in the Earth's atmosphere altering the Earth's energy balance by playing a dominant role in the atmospheric thermal opacity and having a major amplifying influence on several factors of anthropogenic climate change through various feedback mechanisms (Kiehl and Trenberth, 1997; Randall et al., 2007; Trenberth et al., 2009). Though its great importance not only on processes on global/climate scale, the complex interactions between the components of the hydrological cycle (including water vapour) and the atmosphere are still one of major challenges of climate modelling and for a better understanding of the Earth's climate system in general (Stevens and Bony, 2013). Moreover, the amount and distribution of water vapour are highly variable, so that for global observations these must also be measured with high spatiotemporal resolution. Considering that changes in water vapour are closely linked to changes in temperature via the Clausius-Clapeyron equation, i.e. for typical atmospheric conditions a temperature increase of 1 K yields an increase in the water vapour concentration by approximately 6-7% (Held and Soden, 2000), it is essential to monitor the variability and change of the amount and distribution of water vapour on global scale accurately.

To observe the water vapour distribution on global scale, satellite measurements provide invaluable information. Due to its spectroscopic absorption properties, water vapour can be retrieved from satellite spectra in various different spectral ranges, ranging from the radio (e.g. Kursinski et al., 1997), microwave (e.g. Rosenkranz, 2001), thermal infrared (e.g. Susskind et al., 2003))(e.g. Susskind et al., 2003; Schlüssel et al., 2005; Schneider and Hase, 2011), short and near-infrared (e.g. Bennartz and Fischer, 2001; Gao and Kaufman, 2003) (e.g. Bennartz and Fischer, 2001; Gao and Kaufman, 2003; Schrijver et al., 2009; Dupuy et al., 2016; Schneider et al., 2020) to the visible spectral range (e.g. Noël et al., 1999; Lang et al., 2003; Wagner et al., 2003; Grossi et al., 2015).

Within the past decade, substantial progress has been made to retrieve total column water vapour (TCWV) within the visible blue spectral range (e.g. Wagner et al., 2013; Wang et al., 2019; Borger et al., 2020; Chan et al., 2020) allowing to make use of measurements from satellite instruments like TROPOMI (Veefkind et al., 2012) and even GOME-2 (Munro et al., 2016) for which so far only retrievals in the visible red and near-infrared spectral range have been available. In comparison to these aforementioned spectral ranges, TCWV retrievals in the visible "blue" have several advatanges, for instance similar sensitivity for the near-surface layers over land and ocean due to a more homogenous surface albedo distribution than at longer wavelengths (Koelemeijer et al., 2003; Wagner et al., 2013; Tilstra et al., 2017). Moreover, any satellite mission dedicated to NO_2 monitoring is covering this spectral range.

For investigations of climate change or global warming, respectively, the Ozone Monitoring Instrument (Levelt et al., 2006, 2018) onboard NASA's Aura satellite is particularly interesting: launched in July 2004 it offers an almost continuous measurement data record of more than 16 years up until today. In this study, we make use of OMI's long-term data record and retrieve total

column water vapour (TCWV) from its measurements in the visible blue spectral range in order to generate a climate data set. The paper is structured as follows: in Sect. 2 we describe the data set generation and briefly explain the retrieval methodology and the applied modifications in comparison to the TCWV retrieval from Borger et al. (2020). Then in Sect. 3, we investigate potential sampling errors and how the limitation to clear-sky satellite observations influences the representativeness of the TCWV values of the data set. Furthermore, in Sect. 4 we characterize the data set via a validation study an intercomparison to the various different reference TCWV data sets and also analyze its temporal stability in Sect. 5. Finally, we briefly summarize our results in Sect. 6 and draw conclusions.

2 OMI TCWV data set

2.1 Ozone Monitoring Instrument

The Ozone Monitoring Instrument OMI (Levelt et al., 2006, 2018) onboard NASA's Aura satellite is a nadir-looking UV-vis pushbroom spectrometer that measures the Earth's radiance spectrum from 270–500 nm with a spectral resolution of approximately 0.5 nm following a sun-synchronous orbit with an equator crossing time around 13:30 LT. The instrument employs a 2D CCD consisting of 60 across-track rows which in total cover a swath width of approximately 2600 km with a spatial resolution of 24 km × 13 km at nadir increasing to 24 km × 160 km towards the edges of the swath. Launched in July 2004, OMI provides an almost continuous measurement record until today with more than 90000 orbits.

However, since July 2007 OMI has suffered from the so-called "row-anomaly" (RA), a dynamic artefact causing abnormally low radiance readings in the across-track rows, i.e. several rows of the CCD detector receive less light from the Earth, and some other rows appear to receive sunlight scattered off a peeling piece of spacecraft insulation. One plausible explanation for these effects is a partial obscuration of the entrance port by insulating layer material that may have come loose on the outside of the instrument (Schenkeveld et al., 2017; Boersma et al., 2018). Thus, in this study, the affected measurements are excluded for the entire period of the evaluationdata set.

2.2 Methodology and modifications of the spectral analysis

To retrieve total column water vapour (TCWV) from UV-vis spectra from OMI, we apply the TCWV retrieval of Borger et al. (2020) developed for the TROPOspheric Monitoring Instrument (TROPOMI) onboard Sentinel-5P. The retrieval is based on the principles of Different Optical Absorption Spectroscopy (DOAS, Platt and Stutz, 2008) with a fit window between 430–450 nm and consists of the common two-step DOAS approach: first, the absorption along the light path is calculated:

$$\ln\left(\frac{I}{I_0}\right) \approx -\sum_i \sigma_i(\lambda) \cdot \mathrm{SCD}_i + \Psi + \Phi \tag{1}$$

where I and I_0 and I represent the solar irradiance and the radiance backscattered from Earth, respectively, and i denotes the index of a trace gas of interest, $\sigma_i(\lambda)$ its respective molecular absorption cross section, $\mathrm{SCD_i} = \int_s c_i ds$ its concentration integrated along the light path s (the so called slant column density), Ψ summarizing terms accounting for the Ring effect and additional pseudo-absorbers, and Φ a closure polynomial accounting for Mie and Rayleigh scattering as well as parts of the low-frequency contributions of the trace gas cross sections.

Second, to convert the slant column density to a vertical column density (VCD), we apply the so called airmass factor (AMF):

$$\mathrm{VCD} = \frac{\mathrm{SCD}}{\mathrm{AMF}} \tag{2}$$

The AMF accounts for the non-trivial effects of atmospheric radiative transfer and depends on the conditions of the retrieval scenario (i.e. aerosol and cloud effects, viewing geometry, and surface properties) as well as the profile shape of the trace gas of interest. The algorithm of Borger et al. (2020) makes use of the relation between the H_2O VCD and the profile shape and iteratively finds the optimal VCD by assuming an exponential water vapour profile shape.

For the application of the algorithm to OMI measurements several modifications had to be applied to the algorithm of Borger et al. (2020). For climate studies such as trend analyses it is evident to provide a consistent data record. Thus, all rows that have ever been affected by the so called "row-anomaly" are excluded from the data set for the complete time series, which corresponds to approximately half of the OMI swath. Also, instead of a daily solar irradiance an Earthshine radiance is used as reference spectrum within the DOAS analysis. The rationale for using an Earthshine radiance over a solar irradiance is as follows:

- The daily OMI solar irradiance spectra (OML1BIRR version 3) are very noisy and have several gaps causing high H_2O SCD fit errors and thus leading to an overall poor quality of the H_2O VCD data set.
- By using an annual mean solar irradiance spectrum from the year 2005 (also used during the QA4ECV project; Boersma et al., 2018) a good fit quality can be obtained, however, OMI is also suffering from degradation effects (Schenkeveld et al., 2017). Thus, for the case of climate trend analyses it will be almost impossible to disentangle if a trend signal originates from the spectral degradation of OMI or indeed from a geophysical trend (see also Fig. A1). By using an Earthshine radiance as reference spectrum these degradation effects will largely cancel out.
- By using an Earthshine radiance as reference spectrum, also the across-track biases within the OMI swath are strongly reduced (see Panel (c) in Fig. 1) and consequently no destriping is necessary during post-processing (see also Anand et al., 2015).
- However, as a disadvantage of the use of Earthshine spectra, the retrieved H_2O slant columns do not represent absolute slant columns because the Earthshine reference spectra also contain H_2O absorptions. Hence, a slant column representative for the chosen reference sector has to be added to the retrieved values.

For the creation of annual Earthshine reference spectra we selected the Antarctic continent as reference sector (high surface albedo due to snow and ice cover) and the time period of December (i.e. during austral summer) yielding a relatively high signal-to-noise ratio for our radiance measurements despite large solar zenith angles. Furthermore, only pixels above an altitude of 2000 m above sea level are selected: as the air temperatures are very low there, the water vapour concentrations are very low as well, thus representing a reference atmosphere that is as dry as possible (i.e. the reference SCD or better saying the absolute value of its uncertainty has to be as minimal as possible). Also, to avoid the inclusion of noisy measurements (in particular from the descending part of the OMI orbit), only pixels with a solar zenith angle (SZA) $< 80°$ are considered. From these measurements we calculate the monthly-mean radiance for December for each year for every OMI row and then use the resulting reference spectra for the retrievals of the upcoming year.

Figure 1 illustrates the effect of different reference spectra on the H_2O SCD distribution for an examplary orbit. Distinctive stripe patterns are prominent in particular when using the daily solar irradiance as reference spectrum (Panel (a) in Fig. 1). Although the usage of the annual-mean solar irradiance (Panel b) can reduce the strength of the stripes, they are still clearly visible. In contrast, no across-track stripes are detectable for the case of the Earthshine reference and overall the SCDs are also lower due to the H_2O absorption in the Earthshine reference (Panel c).

Further details about destriping in general and a comparison of the temporal behaviour of the irradiance based and Earthshine SCD are available in Appendix A.

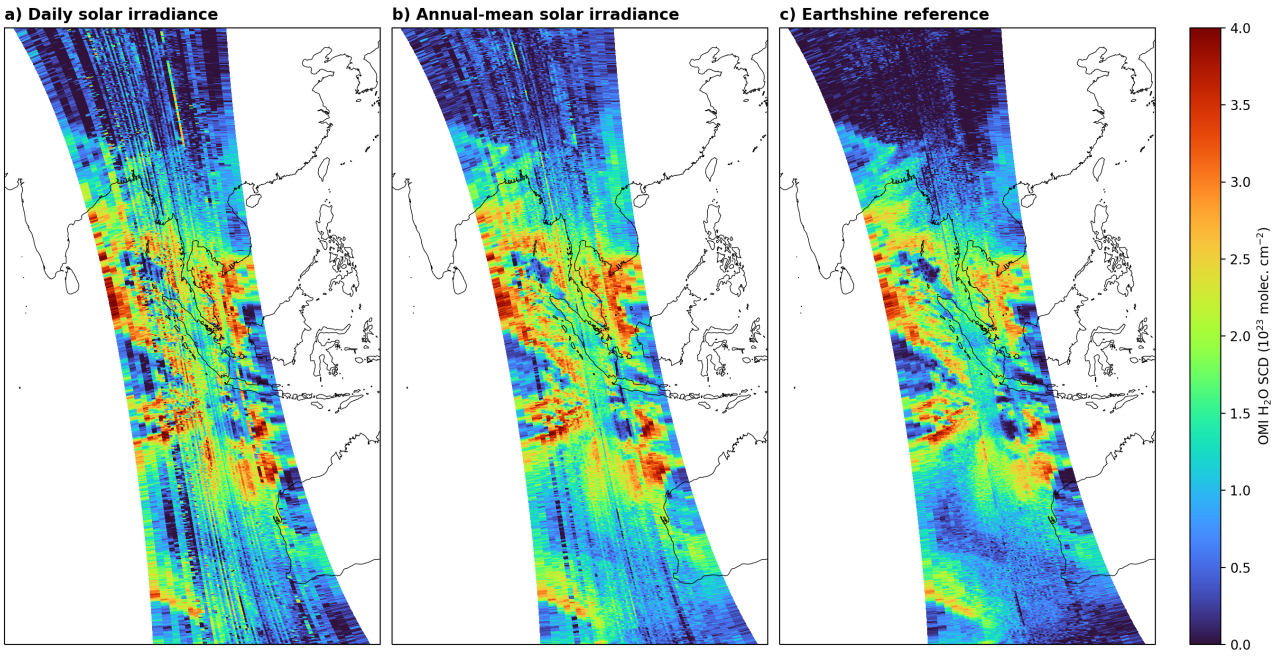

Figure 1. Examplary orbit showing the impact of different reference spectrum on the OMI H_2O SCD distribution: a) daily solar irradiance, b) annual-mean solar irradiance, and c) monthly mean Earthshine reference. Orbit 34382, date 01-01-2011.

2.3 VCD conversion and data set generation

To account for the potential water vapour contamination within the Earthshine reference spectra, the SCDs based on the Earthshine reference have to be corrected for the corresponding offset. In this study, we determine this offset ΔSCD for each row based on the difference of the Earthshine based SCDs and solar irradiance based SCDs for the first 5 years of OMI operation (see Appendix A). Equation (2) can then be rewritten as:

$$\mathrm{VCD} = \frac{\mathrm{eSCD} + \Delta\mathrm{SCD}}{\mathrm{AMF}} \tag{3}$$

where eSCD denotes the SCD derived using the Earthshine reference.

The AMFs are calculated as described in Borger et al. (2020). For the determination of the AMF, additional information about the retrieval scenario like cloud cover and surface properties is necessary. We use the cloud information from the OMI L2 NO_2 product (OMNO2, Lamsal et al., 2021) and the modified OMI surface albedo version of Kleipool et al. (2008) as described in Borger et al. (2020). We also tested the surface albedo information from the OMNO2 product, however, within the framework of a trend analysis study (?) (Borger et al., 2022) we observed spatial artefacts in the surface albedo trends which likely arise

from the use of an older version of the MODIS data for the albedo calculation (Lok Lamsal, personal communication). The distribution of TCWV trends is mainly determined by the trends in the SCD. The albedo or AMF trends usually only determine whether the trend signal becomes stronger or weaker, but this only affects trends over land, since an albedo climatology from Kleipool et al. (2008) is used over ocean. As the ice flags from the OMI processor sometimes indicate snow/ice-free surfaces over Antarctica or Greenland, we additionally use the monthly mean sea ice cover information from ERA5 (Hersbach et al., 2020) and the annual mean land cover information from MODIS Aqua (Sulla-Menashe et al., 2019).

To create the OMI TCWV data set, we have chosen the time range from January 2005 to December 2020 and only include observations with an effective cloud fraction $< 20\%$ and AMF > 0.1. Furthermore, the pixels have to be free of snow and ice and must not be affected by the row anomaly. So while about 50% of the orbit is missing because of the RA-filter, the remaining data still cover an "effective" swath of about 1300 km and is thus still larger than the swaths of GOME-1, SCIAMACHY, or GOME-2A (all about 1300 km) or of the order of SSM/I (about 1394 km). Thus, OMI still achieves complete coverage of the Earth about every 2-3 days, which should provide enough observational data for good representativeness in case of a monthly mean (see also Appendix C and the good agreement to the reference data in Sect. 4). In total, this leaves about 30% of TCWV dat afrom an RA-filtered orbit and about 12% of data from a complete orbit. The results of every orbit are then gridded to a $1° \times 1°$ lattice for every day. From these daily grids, the monthly mean H_2O VCD distributions are then calculated ensuring that a continuous TCWV time series is available for as many grid cells as possible.

Figure 2 shows the global mean OMI H_2O VCD averaged over the complete time range of the TCWV data set. The resulting distribution demonstrates that the retrieval is capable to capture the macroscale water vapour patterns like high VCD values in the tropics (in particular over the maritime continent) and low values towards the polar regions, but also characteristic regional patterns like the South Pacific convergence zone.

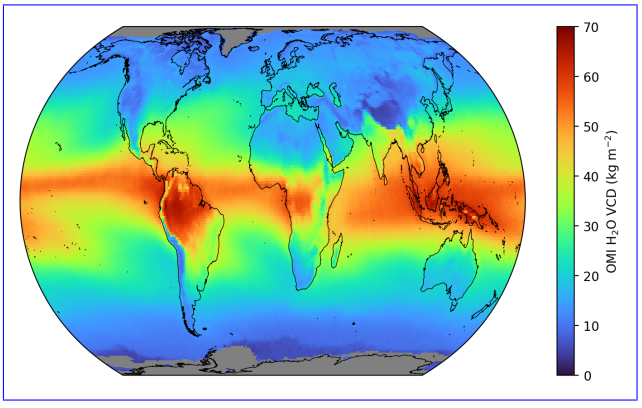

Figure 2. Global mean OMI H_2O VCD distribution from 2005 until 2020 based on the OMI analysis using Earthshine reference spectra and corrected for the H_2O SCD bias. Areas with no valid values are coloured grey.

3 ValidationSampling errors and clear-sky bias

Although satellite observations enable the analysis of trace gas concentrations on global scale, a fundamental problem is that typically a satellite measurement is only taken once a day for one location. Furthermore, satellite measurements are usually only available under cloud-free conditions, especially in the visible or infrared spectral range and thus no continuous time series is guaranteed. Consequently, they cannot provide a complete picture of geophysical variability, which leads to sampling errors in the calculation of averaged values (e.g. monthly means).

Moreover, the question arises to what extent the limitation to cloud-free pixels influences the monthly averages determined from the OMI satellite measurements, i.e. whether in the OMI TCWV data set a so-called "clear-sky bias" exists. Gaffen and Elliott (1993) investigated this bias using radiosonde ascents and found that the TCWV is about 0-15% lower under cloud-free conditions than under cloudy conditions. Similarly, Sohn and Bennartz (2008) found a clear-sky bias between MERIS and AMSR-E of about 10%.

To estimate the sampling errors, we follow the methods of Xue et al. (2019) and Gleisner et al. (2020): we choose hourly-resolved ERA5 data with a spatial resolution of $0.25° \times 0.25°$ as reference data and collocate the ERA5 data with OMI overpass times. These data are then resampled to the $1° \times 1°$ resolution of the OMI TCWV data set and the monthly averages are calculated ($\mathrm{TCWV}_{\mathrm{sampled}}$). We then take the complete, original ERA5 data, resample it to the same spatial resolution and calculate monthly means from this data as well ($\mathrm{TCWV}_{\mathrm{true}}$). The difference between the two data sets then represents the sampling error:

$$\varepsilon_{\mathrm{sampling}} = \mathrm{TCWV}_{\mathrm{sampled}} - \mathrm{TCWV}_{\mathrm{true}} \tag{4}$$

With this definition, the sampling error summarises the uncertainties due to gaps in the swath, temporal differences or missing data (e.g. due to clouds) (Xue et al., 2019).

Figure 3 shows the mean absolute and relative sampling errors for the complete time range of the OMI TCWV data set (January 2005 to December 2020). Overall, it can be seen that most deviations are negative, i.e. the actual TCWV is underestimated. Regarding the absolute deviations, the strongest deviations can be seen in the area of storm-tracks in the mid-latitudes (e.g. North Atlantic) and the polar regions with values around $-5\,\mathrm{kg\,m^{-2}}$. The smallest deviations are found in the quasi-permanent cloud-free regions in the subtropics. As expected, the relative differences increase from the equator towards the poles due to the decreasing TCWV values and reach values stronger than -30%.

To investigate to what extent these deviations are related to the clear-sky bias, we proceed similarly to the calculation of the sampling error: we collocate the ERA5 data to the OMI overpass time and once apply a cloud filter (effective cloud fraction < 20%) and once not. Then we resample both data sets to $1° \times 1°$ and calculate monthly means. The difference of both data sets then represents the clear-sky bias:

$$\varepsilon_{\mathrm{clear}} = \mathrm{TCWV}_{\mathrm{clear}} - \mathrm{TCWV}_{\mathrm{all}} \tag{5}$$

To determine seasonal structures, the global distributions of the absolute and relative clear-sky bias for the different seasons were determined from the monthly differences (see Fig. 4). Overall, the distributions of the clear-sky bias correspond

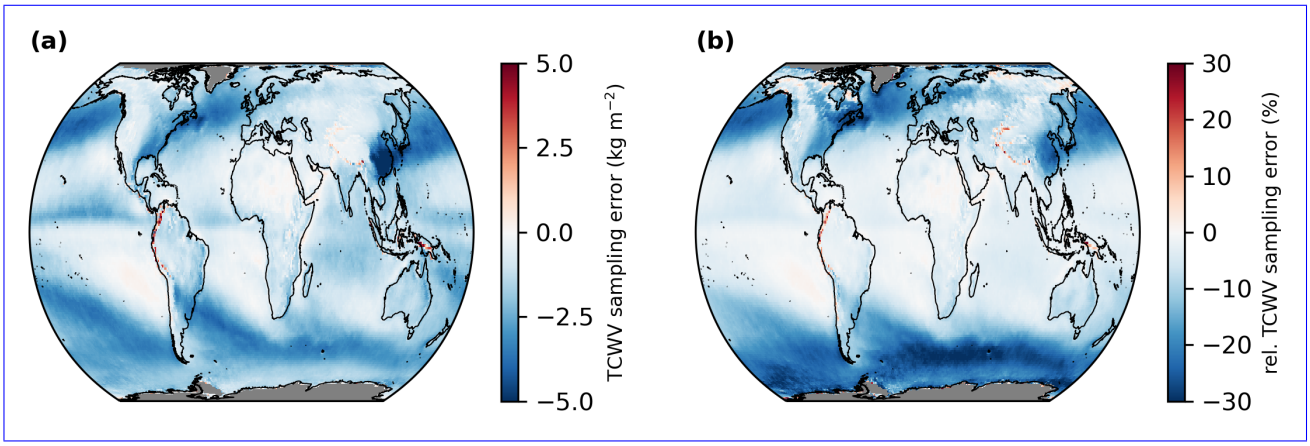

Figure 3. Global distributions of the mean sampling errors derived from monthly mean sampling differences for the time range January 2005 to December 2020. Panel (a) depicts absolute sampling error (i.e. $\varepsilon_{sampling}$) and Panel (b) relative sampling error (i.e. $\varepsilon_{sampling}/\mathrm{TCWV_{true}}$). Grid cells for which no data is available are coloured grey.

very closely to the distributions of the sampling error, both in strength and in pattern. Moreover, the absolute and relative deviations show only slight changes between the different seasons.

Figures 5 and 6 summarize the sampling error and clear-sky bias distributions, respectively. For the sampling error we obtain a mean absolute deviation of –1.6 kg m^{-2} (median –1.4 kg m^{-2}) and a mean relative deviation of -9.5% (-6.2%) and for the clear-sky bias we get a mean absolute deviation of –1.7 kg m^{-2} (median –1.3 kg m^{-2}) and a mean relative deviation of -10.0% (-5.9%). However, the distributions of the absolute and relative deviations for the sampling error and the clear-sky bias are highly left-skewed and thus the mean value in particular is influenced by the long tails of the distributions. Nevertheless, for the clear-sky bias the obtained values agree well with the findings of Gaffen and Elliott (1993) and Sohn and Bennartz (2008).

Since the effect of the clear-sky bias is already included in the sampling error and the results for both errors are very similar, it can be assumed that the spatial and temporal sampling errors play only a minor or negligible role compared to the clear-sky bias.

In addition to the sampling error and the clear-sky bias, we also examined in Appendix C to what extent the monthly means would change if no RA-filter is applied, i.e. if all data of the complete OMI swath were available. It turns out that although deviations arise due to the RA-filter, these deviations are almost an order of magnitude smaller than those of the clear-sky bias and the global distribution of the deviations is mostly noisy. Due to this small influence of the RA-filter, we conclude that the filtered OMI TCWV data are a good representation of the actual TCWV values.

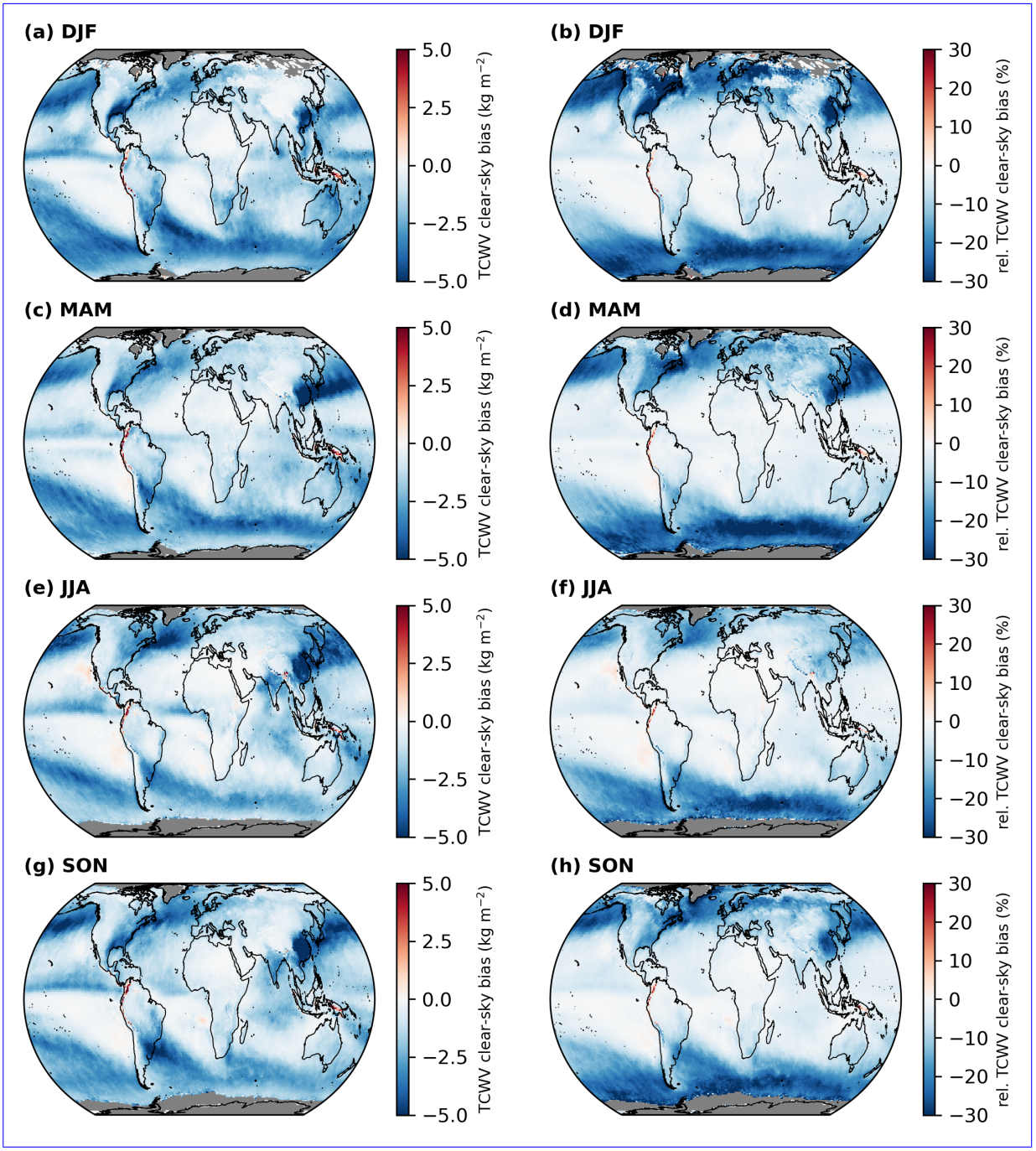

Figure 4. Global distributions of the absolute differences (ε_{clear}; left column) and relative differences ($\varepsilon_{clear}/\mathrm{TCWV_{all}}$; right column) of the mean differences between clear-sky and all-sky ERA5 based on the OMI cloud information for winter (DJF; a & b), spring (MAM, c & d), summer (JJA, e & f), and autumn (SON, g & h) for the time range January 2005 to December 2020. Grid cells for which no data is available are coloured grey

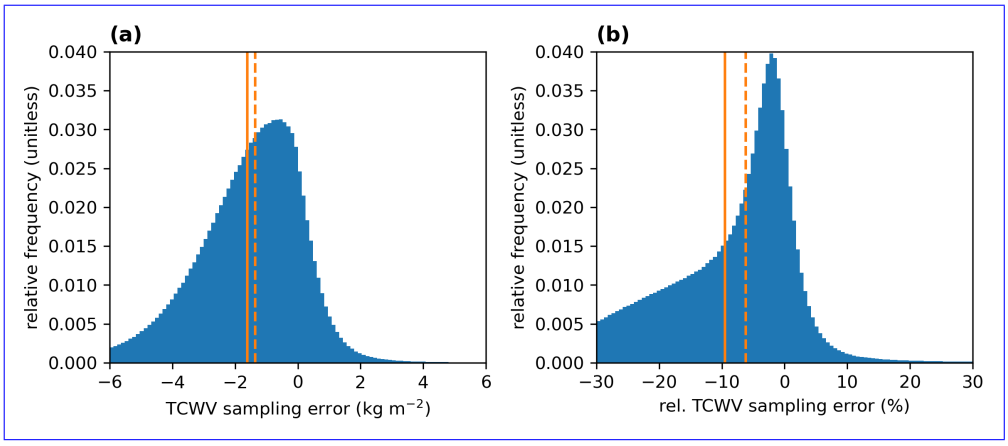

Figure 5. Distributions of the absolute differences ($\varepsilon_{sampling}$; Panel a) and relative differences ($\varepsilon_{sampling}/\mathrm{TCWV_{true}}$; Panel b) of the monthly mean differences between clear-sky and all-sky ERA5 data based on the OMI cloud information. The solid and dashed orange line indicate the mean and the median of the distributions, respectively.

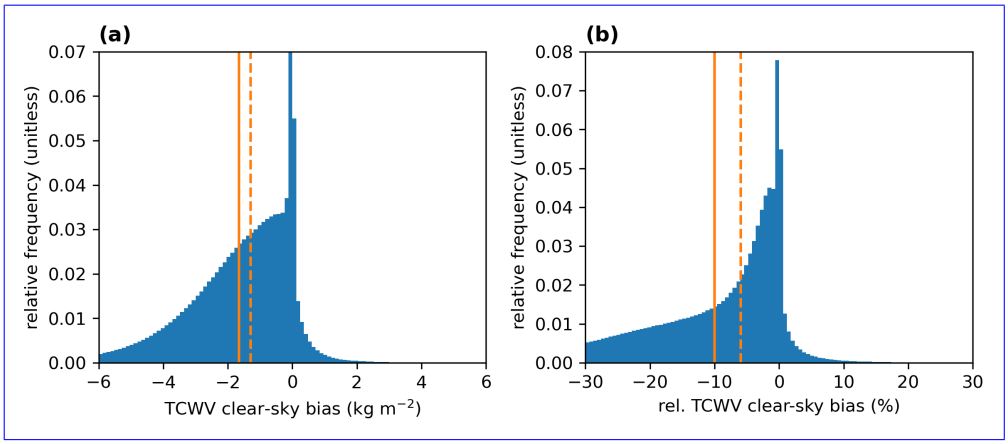

Figure 6. Distributions of the absolute differences (ε_{clear}; Panel a) and relative differences ($\varepsilon_{clear}/\mathrm{TCWV_{all}}$; Panel b) of the monthly mean differences between clear-sky and all-sky ERA5 data based on the OMI cloud information. The solid and dashed orange line indicate the mean and the median of the distributions, respectively.

4 Intercomparison to existing water vapour climate data records

To evaluate the overall quality of the OMI TCWV data set, we conducted a validation an intercomparison study for which we use the merged, 1-degree total precipitable water (TPW) data set version 7 from Remote Sensing Systems (RSS) (Mears et al., 2015; Wentz, 2015), TCWV data from the reanalysis model ERA5 (Hersbach et al., 2019, 2020), and the ESA WaterVapour CCI _Vapour_CCI (WV_cci) climate data record CDR-2 as reference. For the correlation analysis we perform an ordinary least-squares (OLS)linear regression and

The RSS data set consists of merged geophysical ocean products whereby the values are retrieved from various passive satellite microwave radiometers. These microwave radiometers have been intercalibrated at the brightness temperature level and the ocean products have been produced using a consistent processing methodology for all sensors (more details in Wentz, 2015; Mears et al., 2015). The major advantages of microwave TCVW retrievals are their high precision and accuracy and that they are insensitive to clouds, so that TCWV values can also be retrieved even under cloudy-sky conditions. A disadvantage, however, is that these retrievals are (mostly) only available over the ocean surface.

Thus, we also compare the OMI TCWV data to the ESA WV_cci CDR-2. At the moment of preparation of this manuscript, the CDR-2 is a beta-version of the combined microwave and near-infrared imager based TCWV data record (COMBI). The CDR combines microwave and near-infrared imager based TCWV over the ice-free ocean as well as over land, coastal ocean and sea-ice, respectively. The data record relies on microwave observations from SSM/I, SSMIS, AMSR-E and TMI, partly based on a fundamental climate data record (Fennig et al., 2020) and on near-infrared observations from MERIS, MODIS-Terra and OLCI (Danne et al., 2022).

Within comparisons between different satellite data sets a major drawback is the influence of sampling errors due to different observation times, pixel footprint sizes or orbit patterns. To minimise this source of error, data from reanalysis models are useful. ERA5 is the fifth generation ECMWF reanalysis (Hersbach et al., 2020) and combines model data with in situ and remote sensing observations from various different measurement platforms. For our purpose, we use the "monthly averaged reanalysis by hour of day" from the Copernicus Climate Data Store on a $1° \times 1°$ grid. To account for OMI's observation time (around 13:30 LT), we first calculate the local time for each longitude in the ERA5 data set, then select the TCWV data for the time period between 13:00-14:00 LT and finally merge the selected data.

For the intercomparison, it is also important to consider that the reference data sets are not perfect or error-free and that the comparisons across the different TCWV regimes are not consistent. Thus, we perform an orthogonal distance regression (ODR(ODR; Cantrell, 2008) and a piece-wise linear regression (PWLF). In the case of the ODR it is necessary to use reasonable ratios of the relative errors of the compared data sets instead of using absolute errors in order to obtain meaningful results. Mears et al. (2015) found that the uncertainty of daily microwave TCWV observations for TCWV = 10 kg m^{-2} was around 1 kg m^{-2} and for TCWV = 60 kg m^{-2} around 2–4 kg m^{-2}. Hence, we assume that the uncertainty of the RSS data set is 5% or at least 1 kg m^{-2}. For ERA5 and ESA CDR-2 we can assume similar uncertainties over ocean, since the TCWV values there are also mainly based on microwave observations. Unfortunately, no uncertainties are provided for TCWV over land. Thus, for the sake of simplicity, we assume that the relative errors of the reference data sets

over ocean are 5%, over land land are twice as high as over ocean, i.e. 10% , and for or at least 2 kg m^{-2}. For the OMI TCWV data set we assume an uncertainty of 20% (Borger et al., 2020), but at least 2 kg m^{-2}. We also tested other variants of error assumptions and it turned out that the exact choice of errors is negligible for the regression results as long as the ratio of uncertainties remains similar.

4.1 Intercomparison to RSS SSM/I

The RSS data set consists of merged geophysical ocean products whereby the values are retrieved from various passive satellite microwave radiometers. These microwave radiometers have been intercalibrated at the brightness temperature level and the ocean products have been produced using a consistent processing methodology for all sensors (more details in Wentz, 2015; Mears et al., 2015). The left panel in Fig. 7 results of the intercomparison between OMI and the RSS TCWV data set are summarized in Figure 7. Figure 7a depicts the 2D histogram from the comparison between the monthly mean values from RSS and the OMI TCWV data set. The data is distributed closely along the 1-to-1 diagonal (black dashed line) and yields a correlation coefficient of $R = 0.98$. The results of the linear (OLS, red solid line) and orthogonal distance regression (ODR, red dashed line) both solid line) indicate an overall very good agreement with slopes of 1.03 and 1.05, respectively. The right panel of Fig. 7 around 1.01. For the PWLF regression, similar results with a slope around 1.04 are obtained for TCWV values > 9.5 kg m^{-2}, which represents the vast majority of the comparison set (approximately 90%).Figure 7b illustrates the zonally averaged monthly mean difference of OMI minus RSS TCWV within the latitude-time space. In general, the deviations between OMI and RSS are quite low with values between ±2.5 kg m^{-2}. Nevertheless, within a positive bias of +1.0±1.5 kg m^{-2}. Within the tropics (i.e. between −20 to 20 °N) , we obtain a mean deviation of +2.0±1.6 kg m^{-2} and in the extratropics values of +0.7±1.3 kg m^{-2}. However, within the tropics, also distinctive periodic patterns of positive deviations are observable.

Figure 8 shows the global mean TCWV difference between OMI and RSS SSM/I over the complete time period of the OMI TCWV data set. Consistent with the findings from Fig. 7 highest positive deviations can be found in the tropical Pacific ocean and near the coastlines of South America, Africa, and Indonesia whereas strongest negative deviations are obtained around the South Pacific convergence zone and East Siberian Sea. In the case of the tropical Pacific ocean the distribution of the systematic positive deviations matches quite well regions of cold water or of the so called "cold tongue" which is frequently affected by low clouds. Since the highest water vapour concentrations occur in the lower troposphere, small deviations of a few 100 m in cloud height can have relatively large effects on the AMF. In the case of Central America or Atlantic ocean, a too low albedo due to additional absorption by phytoplankton (Kleipool et al., 2008) could explain the systematic positive deviations. Additional comparisons taking into account only valid grid cells according to the "common-mask" from ESA WVCCI CDR _cci are presented in Appendix B. This mask filters regions where no continuous time series of data is available or where the data are affected by high uncertainties e.g. due to frequent cloud cover. If these regions are removed and therefore Therefore only high quality measurements are compared to each other, we obtain a much better agreement to the reference data set and the slight overestimation of 3-5% is reduced to 1-3%. However, since mainly regions over land surface are affected, the comparisons with the filtered data are almost identical to the unfiltered data.

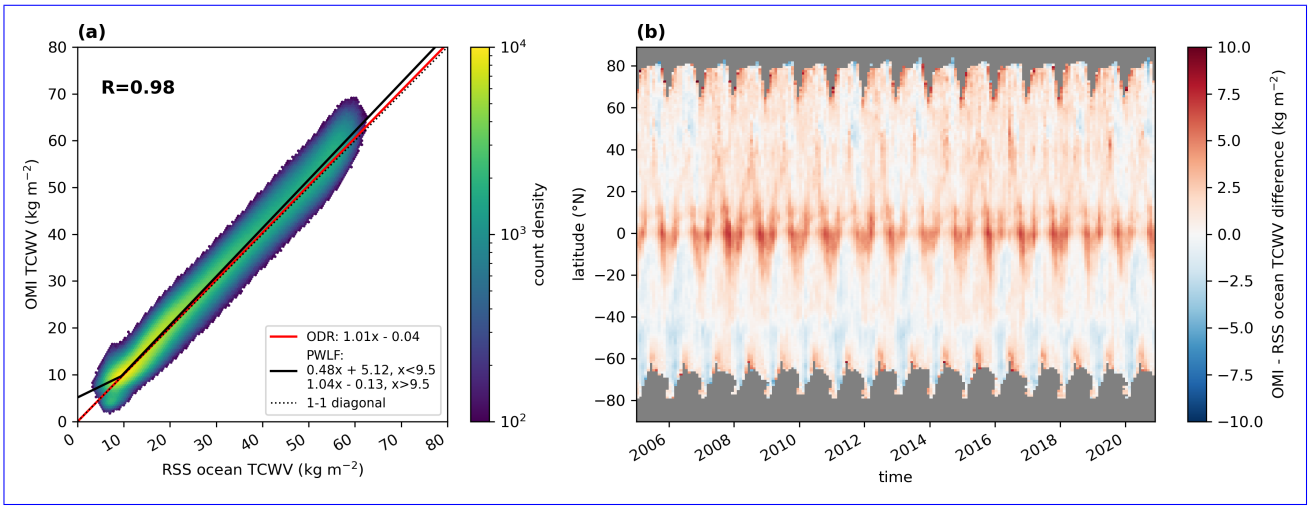

Figure 7. Intercomparison between monthly mean TCWV from OMI and Remote Sensing Systems (RSS) merged SSM/I data set for data over ocean. Left panel: Panel (a) illustrates a 2D histogram in which the colour indicates the count density; the red solid line represents the results of the linear orthogonal distance regression (OLSODR) and the red dashed solid black line the results of the orthogonal distance piecewise linear regression (ODRPWLF). The results of the respective fits are given in the bottom right box and the correlation coefficient in the top left corner. The dashed black line indicates the 1-to-1 diagonal. Right panel: Panel (b) depicts the TCWV difference of OMI - minus RSS within the latitude-time space; reddish colours indicate an overestimation, blueish colours an underestimation of the OMI TCWV data set.

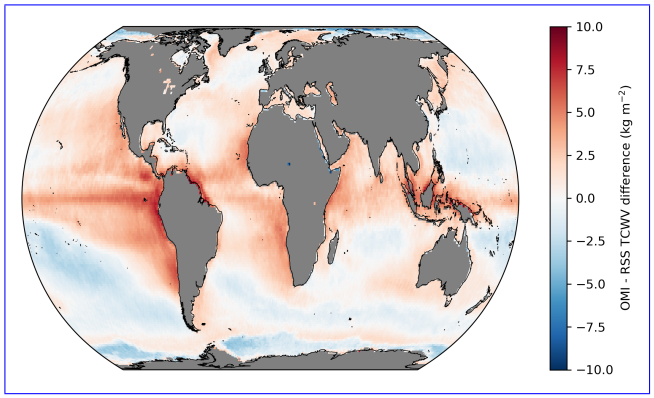

Figure 8. Global mean TCWV difference of OMI minus RSS SSM/I for the time range January 2005 until December 2020. Areas with no valid values are coloured grey.

4.2 Intercomparison to ERA5

For further validations, we also compare the OMI TCWV data to ERA5 (Hersbach et al., 2020). To account for OMI's observation time (around 13:30 LT), we only take into account ERA5 monthly mean values between 13:00-14:00 LT. The results of the intercomparison to ERA5 are depicted in Figure 9. To investigate

potential dependencies on the surface type, we separated the data into data over ocean (top row in Fig. 9a & b) and data over land (bottom row in Fig. 9c & d). The intercomparison for data over ocean reveals similar results as the intercomparison between OMI and RSS: the results of the OLS and ODR ODR results indicate a slight overestimation (slopes of around 1.05 and 1.081.03) together with a correlation coefficient close to unity (R of around 0.98). Moreover, the periodic pattern of positive deviations in the tropics occurs again, with an overall small positive bias of $+1.7 \pm 1.7\,\mathrm{kg\,m^{-2}}$, which increases to $+3.4 \pm 1.7\,\mathrm{kg\,m^{-2}}$ in the tropics (–20 to 20 °N) but is around $+1.1 \pm 1.3\,\mathrm{kg\,m^{-2}}$ in the extratropics.

In contrast, the regression For data over land, the picture is different: although the ODR gives similar results for the intercomparison slope as for data over land reveal a distinctive overestimation by about 11% for the OLS and slightly less for the ODR (8%) but still with a high correlation coefficient of 0.97. Interestinglyocean, the distribution in the 2D histogram (bottom left panel in Fig. 9c) shows particularly strong positive deviations of approximately $+10\,\mathrm{kg\,m^{-2}}$ at high TCWV values . Within a piecewise linear regression and an overall systematic offset of around $+1.43\,\mathrm{kg\,m^{-2}}$. Within the PWLF analysis we find a good agreement to the reference data for TCWV values up to about $26\,\mathrm{kg\,m^{-2}}$ $25\,\mathrm{kg\,m^{-2}}$ (which represents approximately 74% of all data points) with slopes of around 0.96. However, for higher TCWV values we find distinctive positive overestimations of up to 26%. 24%. Nevertheless, even for low TCWV values a systematic offset of approximately $+2.52\,\mathrm{kg\,m^{-2}}$ is obtained.

According to the corresponding latitude-time difference plot (bottom right panel in Fig. 9d), the systematic positive deviation in the tropics is now much stronger with values around $+6.2 \pm 3.4\,\mathrm{kg\,m^{-2}}$ (for latitudes $< 20°$), however, in other regions the extratropics the positive deviation is much lower or around $+1.7 \pm 1.2\,\mathrm{kg\,m^{-2}}$ on average and thus of similar magnitude as for the ocean comparisons. Closer inspection of the mean TCWV difference between OMI and ERA5 (see Fig. 10) reveals that the strong deviations over the tropical landmasses mainly occur in the regions that are affected by frequent cloud cover such as the Amazon basin, Central Africa and the maritime continent.

Hence, the reasons for the distinctive positive deviations with respect to ERA5 may arise from different causes. For the case of the OMI TCWV retrieval two main uncertainty sources may cause the strong, systematic positive deviations: First, there is the possibility that the used land surface albedo from Borger et al. (2020) is too low, leading to an underestimation of the AMF and consequently to an overestimation of the H_2O VCD. However, Borger et al. (2020) also showed that their modified albedo map led to overall better results for the case of the TROPOMI TCWV retrieval. On the other hand, there may also be uncertainties in the retrieval input data of the cloud information from L2 NO_2 product: If for example the surface albedo is underestimated in the input of the cloud algorithm, this leads to an overestimation of the cloud top height and thus to an underestimation of the AMF, and finally to an overestimation of the H_2O VCD. For the case of ERA5, the frequent cloud cover can be also major source of uncertainty, as only few satellite measurements (in particular or none at all in the thermal infrared) are available due to the frequent cloud contamination which might lead to clear-sky dry biases in the cloud-affected regions and increased uncertainties within the assimilation process due to the complex radiative transfer in cloudy scenarios (e.g. Li et al., 2016). Likewise, these remote regions are affected by an overall sparseness in the observation density of in situ measurements, so the ERA5 TCWV values are likely to be based mainly on modelled data. Overall, the strong positive deviation of the OMI TCWV data set thus likely results from a combination of an overestimation of the OMI TCWV retrieval and an underestimation of the ERA5 data.

Thus, considering these large uncertainties in the OMI retrieval and that the uncertainties in ERA5 for data over tropical landmasses are not negligible anymore, we conclude that the OMI TCWV data set can well represent the global distribution of the atmospheric water vapour content at least over ocean. Over land, however, the data set should be treated with caution due to the systematic positive deviations from the reference data sets, especially in areas of high TCWV values (i.e. above 26 kg m^{-2}25 kg m^{-2}).

An additional comparison in which particularly critical regions were filtered using the ESA WVCCI CDR _cci "common mask" (see Fig. B1) is given in the Appendix B. When this mask is applied, only high quality measurements are taken into account for the intercomparison. Consequently, the regression results for the comparison over land improve significantly As a result, the extreme overestimations are filtered out and the distribution in the 2D histogram for the overland comparison improves considerably (see Fig. B3), so that the slopes now vary between 0.95 and 1.02, which are a). The slope of the ODR is now around 0.97, which is closer to the results of the piecewise-linear PWLF regression for TCWV < 26 kg m^{-2}25 kg m^{-2}.

4.3 Intercomparison to ESA Water Vapour CCI climate data record

In addition to RSS SSM/I and ERA5 we compare the OMI TCWV data to the ESA Water Vapour CCI For the intercomparison with the ESA WV_cci climate data record CDR-2 . At the moment of preparation of this manuscript, the CDR-2 is a beta-version of the combined microwave and near-infrared imager based TCWV data record (COMBI), whose official release is planned in 2021 by CM SAF. The CDR combines microwave and near-infrared imager based TCWV over the ice-free ocean as well as over land, coastal ocean and sea-ice, respectively. The data record relies on microwave observations from SSM/I, SSMIS, AMSR-E and TMI, partly based on a fundamental climate data record (Fennig et al., 2020) and on near-infrared observations from MERIS, MODIS-Terra and OLCI. For the intercomparison we resampled the CDR from its native spatial resolution ($0.5° \times 0.5°$) to the lattice of the OMI TCWV data set. Furthermore, though the CDR covers a time span from July 2002 to December 2017, we focus on the time period January 2005 to March 2016, as the CDR's difference relative to ERA5 over land is only stable over the MERIS and MODIS period, i.e., from 2002 until March 2016 if looking at clear-sky data. For the sake of completeness, the results for the comparison over the complete time range are depicted in the Appendix-Figures B4 and B5.

Figure 11 summarizes the results of the intercomparison. Not surprisingly, the results for data over ocean (top row in Fig. 11a) are similar to the findings of the RSS SSM/I and ERA5 comparison as measurements from the same (or similar) sensors have been considered: the regression ODR results indicate slight overestimations of around 4-62% with correlation coefficients of around 0.97 and the time-latitude diagram indicates an average deviation of +1.3±1.8 kg m^{-2} (+2.5±1.9 kg m^{-2} in tropics, +0.8±1.5 kg m^{-2} in extratropics). Similar to the intercomparison of ERA5, the intercomparison over land (bottom row in Fig. 11) reveals high overestimations of around 11-14%c) shows roughly similar ODR fit results as over ocean, but here we also find striking positive deviations for high TCWV values and an overall positive offset of 2.41 kg m^{-2}. Again, when applying a piecewise linear regression analysis we obtain good obtaingood agreement with slopes of around 0.94 0.95 for TCWV values to about 26 kg m^{-2} but 25 kg m^{-2} but still a distinctive positive offset of 3.73 kg m^{-2} for low TCWV values and distinctive overestimations of up to 33% for higher TCWV values. This even higher slope , which is even higher than for the comparison to ERA5. Consequently, the systematic deviations are also much stronger (see. Fig. 11d) and reach values of around +7.3±3.6 kg m^{-2} in the tropics,

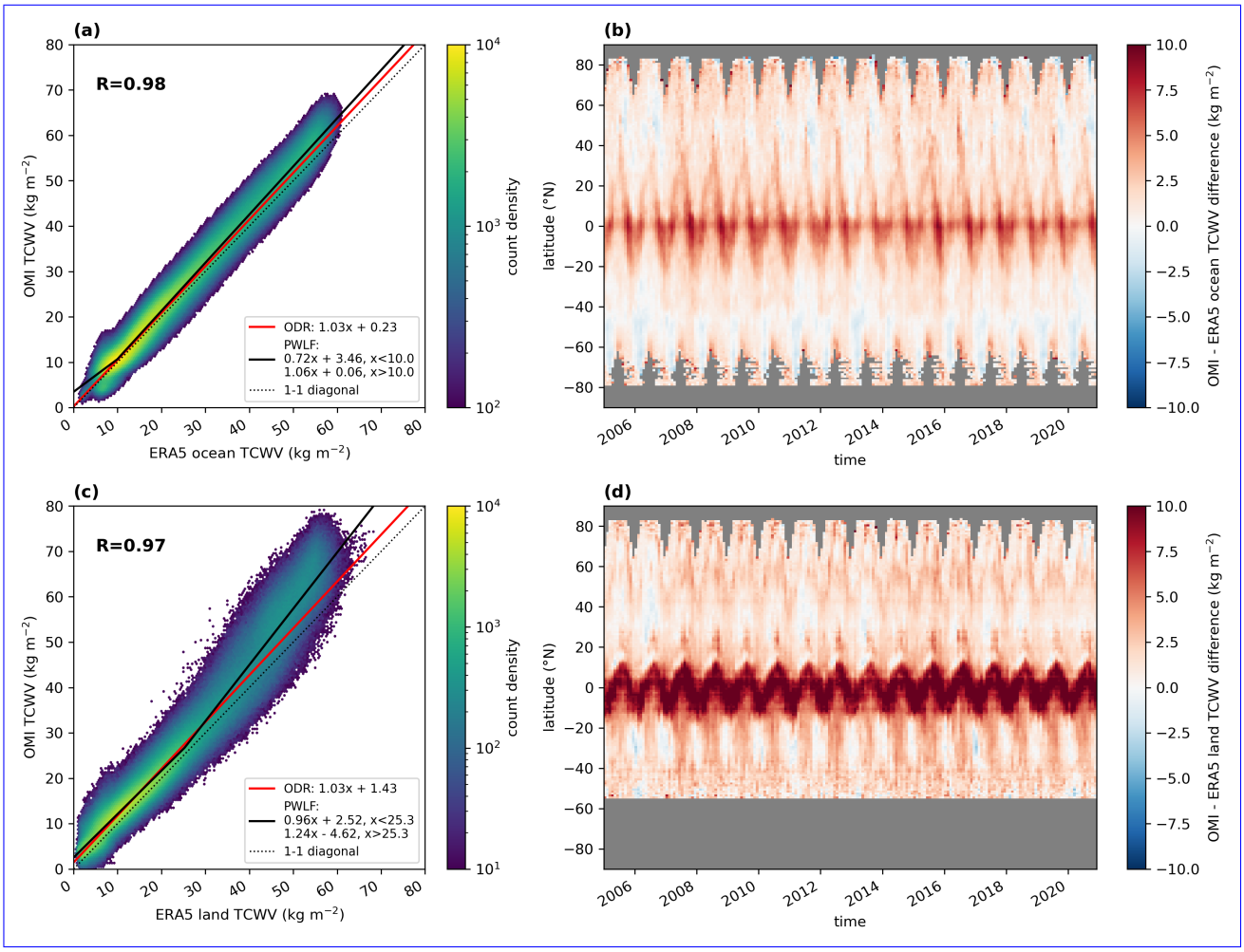

Figure 9. Same as Fig. 7, but now with ERA5 data for data over ocean (top row) and for data over land (bottom row).

around +2.8±1.4 kg m^{-2} in the extratropics, and a global average of +4.2±3.2 kg m^{-2}. These even higher deviations compared to the analysis with ERA5 could be due to the different observation times of the data sets: MERIS on Envisat and MODIS on Terra have an overpass time of 10:00 LT and 10:30 LT, respectively, and follow a descending orbit, whereas OMI measures at 13:30 LT in an ascending orbitwhich could explain the worse agreement.

Overall, similar to the comparison to ERA5 the strongest positive deviations occur again over the tropical landmasses that are mostly affected by frequent cloud cover (see Fig. 12). However, we also observe systematic overestimations along coastlines (e.g. Central America) which eventually arise from sampling issues of the different satellite products and in some mountain regions (e.g. Himalaya) which eventually arise from sampling issues of the different satellite products.

In Appendix B we present a comparison in which critical regions were filtered using the "common mask" from the ESA WV CCI CDR. When this mask is applied, there are clear improvements for the comparison over land: instead of an overestimation of 11-14%,

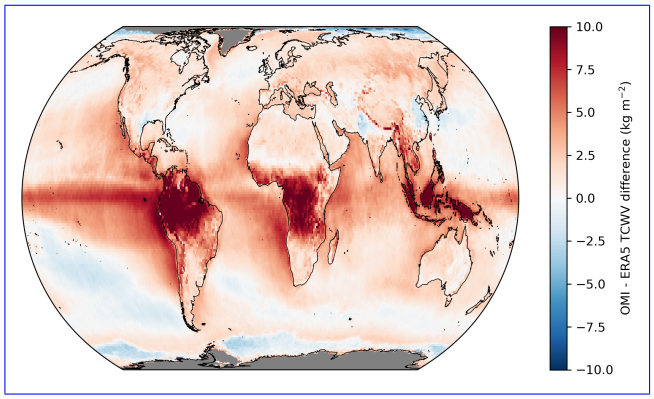

Figure 10. Same as Fig.8, but for ERA5.

a good agreement is obtained with slopes now between 0.97 and 1.04 the prominent overestimates at high TCWV values are filtered out and the distribution is now closer to the 1-1 diagonal (see Fig. B3)b). For the ODR, the slope is around 0.97, which agrees quite well with the slopes obtained for the piecewise linear PWLF regression for TCWV < 26 kg m^{-2}25 kg m^{-2}.

4.4 Temporal stability

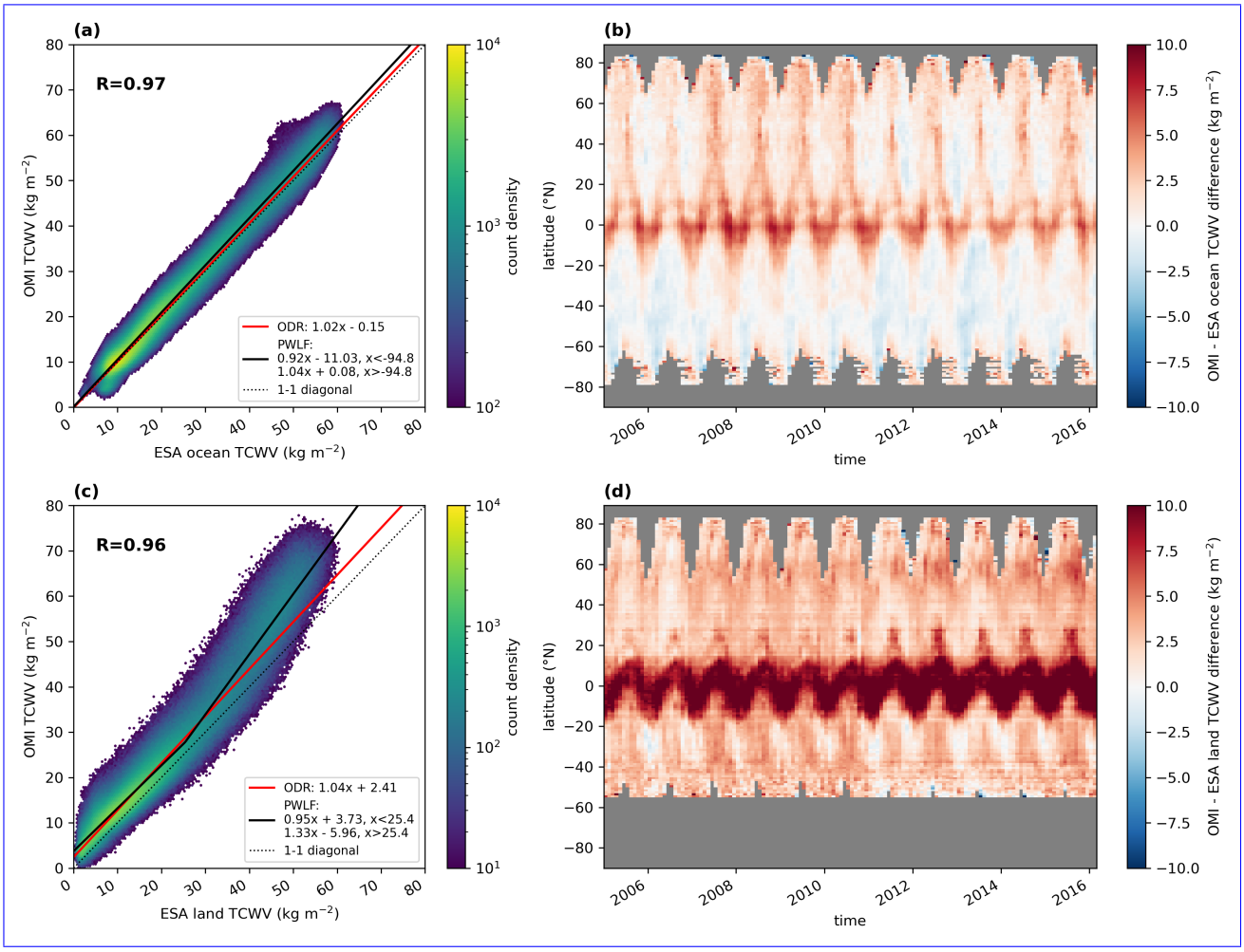

Figure 11. Same as Fig. 7, but now with ESA WV CCI CDR-2 data for data over ocean (top row) and for data over land (bottom row).

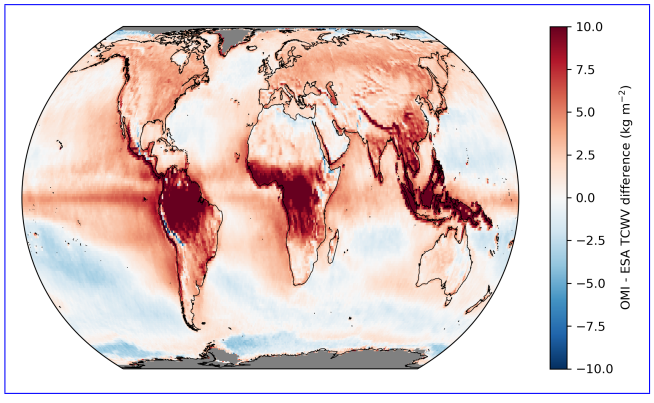

Figure 12. Same as Fig.8, but for ESA WV CCI CDR-2.

5 Temporal stability

In addition to a good agreement to existing reference data sets, the temporal stability is an important property of a climate data record. As the ESA WVCCI _cci CDR data set only covers the time range up to December 2017, we focus on the comparison to the RSS SSM/I and ERA5 data sets as these two cover the complete time range of OMI TCWV data set. For the sake of completeness, however, we also show the results for ESA WVCCI _cci CDR.

To assess the stability of the OMI TCWV data set, we derive the global mean relative deviation $\bar{\epsilon}$ for every time step:

$$\bar{\epsilon} = \frac{\text{mean}\,(\text{OMI} - \text{TCWV}_{\text{ref}})}{\text{mean}\,(\text{TCWV}_{\text{ref}})} \tag{6}$$

and then calculate temporal trends of these deviations using linear ordinary linear least-squares regression following the approach of Danielczok and Schröder (2017) and Beirle et al. (2018) and assess the significance of the results based on a two-sided Student's t-test. For the calculation of global means only data points or grid cells are taken into account for which for every time step data from the OMI TCWV and reference data set are available. In the case of the ESA WVCCI CDR-2 _cci CDR a "common mask" has been provided (see also Fig. B1).

Figure 13 illustrates the temporal variability of the relative differences of the OMI TCWV data set and RSS SSM/I, ERA5, and ESA WVCCI _cci CDR for the time range January 2005 to March 2016 (blue dashed lines) and January 2005 to the end of the respective data set (blue solid lines). For the time series until March 2016 we find trends of +0.80 % dec^{-1} +0.78 % dec^{-1} for the comparison to RSS SSM/I, +0.82 % dec^{-1} for the comparison to ERA5, and −1.00 % dec^{-1} for the comparison to the ESA data. For the time series until the end of the reference data set we find trends of −0.06 % dec^{-1} −0.08 % dec^{-1} for the comparison to RSS SSM/I and −0.18 % dec^{-1} for the comparison to ERA5 and where these trends are not significantly different from 0 % dec^{-1}. For the comparison to the ESA data there is a stronger trend (around −0.52 % dec^{-1}) than for the other two data sets, however also the time range is much shorter and does not cover the complete time range of the OMI TCWV data set. Altogether, the obtained trends of the relative deviations are in line with typical stability requirements for climate data products of ±1 % dec^{-1} (see e.g. Beirle et al., 2018, and references therein)(see e.g. Beirle et al. (2018) and references therein or the ESA WV_cci user requirements; https://climate.esa.int/media/documents/Water_Vapour_cci_D1.1_URD_v3.0.pdf; last access: 26 July 2022).

6 Summary

In this study, we present a long-term 16-year data record of total column water vapour (TCWV) retrieved from multiple years of OMI observations in the visible blue spectral range by means of Differential Optical Absorption Spectroscopy. To derive TCWV from OMI measurements, we applied the TCWV retrieval developed for TROPOMI (Borger et al., 2020) and modified the spectral analysis to account for the degradation of OMI's daily solar irradiance. Thus, annual Earthshine reference spectra were calculated from radiance measurements over Antarctica during December (austral summer).

Within a validation The estimation of the sampling errors in the OMI TCWV data set results in average errors of about -10% (and -6% for the median) and that the largest deviations occur mainly in the the mid-latitude storm tracks and polar regions. Further investigations show that the large deviations of the sampling error correlate well with the deviations of the

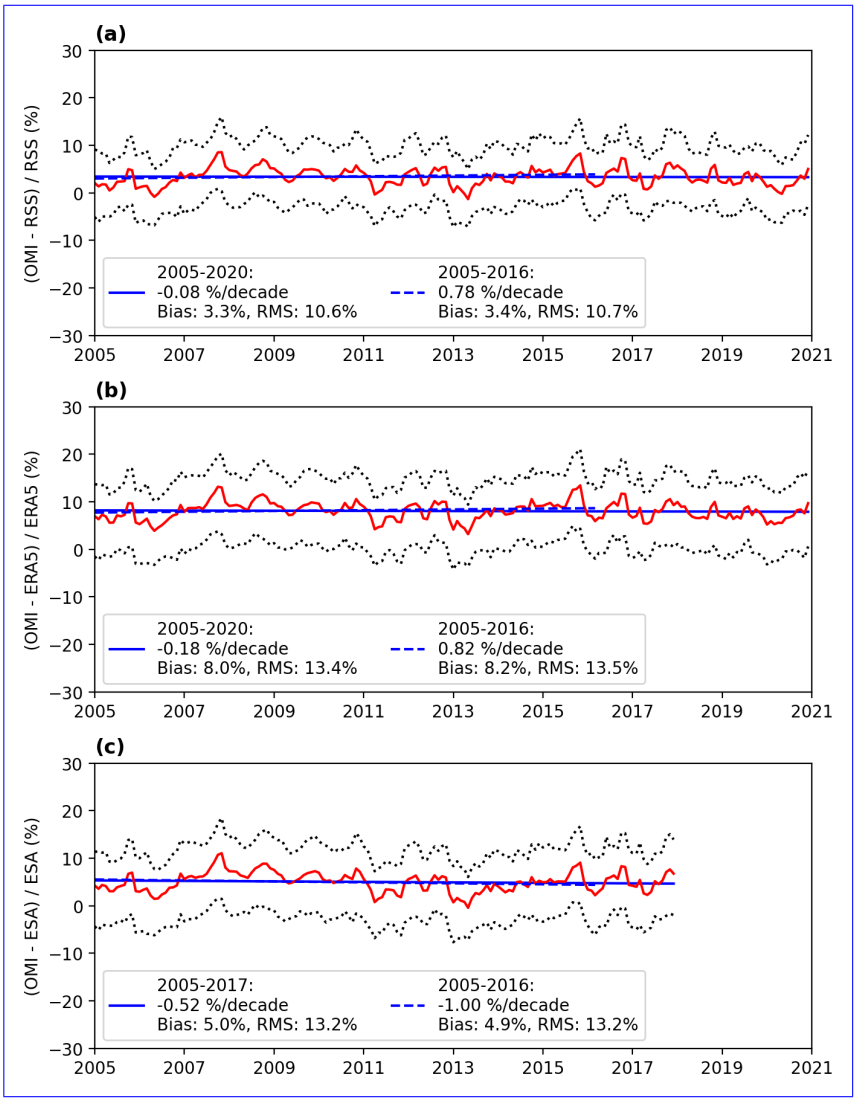

Figure 13. Stability analyses of the global mean relative deviations of the OMI TCWV data set with respect to the ERA5, ESA WV CCI CDR-2, and RSS SSM/I. Red line: global mean relative deviation; blue line: results of linear regression; dotted black line: 25th and 75th percentile, respectively. Dashed lines represent data for the time range from January 2005 to March 2016 and solid lines represent data for the time range from January 2005 to the finish of the respective data set. The bias and RMS provided in the legends correspond to the time seriues of the global mean deviation for the respective time range.

clear-sky bias. However, the investigation of a seasonal effect of the clear-sky bias did not show any seasonal depen-
400 dence. Considering the dominant role of the clear-sky bias on the sampling error, we conclude that the spatiotemporal sampling errors are rather negligible.

Within an intercomparison study, the OMI TCWV data set proves to be in good agreement to the reference data sets of RSS

SSM/I, ERA5, and the ESA WVCCI _cci CDR-2 in particular over ocean surface. However, over land surface the OMI data set systematically overestimates the TCWV content high TCWV values compared to ERA5 and the ESA CDR by approximately 10more than 24% especially in the tropical regions affected by frequent cloud cover. The reasons for these overestimations are manifold, but likely due to an overestimation of the OMI TCWV retrieval due to uncertainties in the retrieval input data (surface albedo, cloud information) on the one hand and an underestimation of the reference data due to missing or uncertain observations on the other hand. Nevertheless, the validation also shows that for TCWV < 26 kg m^{-2} 25 kg m^{-2} good agreement to the reference data can be obtained and also for the case when regions of large uncertainty are filtered. Considering the temporal stability analysis no significant deviation trends could be obtained with respect to ERA5 and RSS SSM/I which demonstrates that the OMI TCWV data set is well suited for climate studies.

Altogether, the OMI TCWV data set provides a promising basis for investigations of climate change: on the one hand, it covers a long time series (more than 16 years and with measurements still in operation), and on the other hand, these measurements are based on a single instrument, so that no bias corrections between different sensors need to be taken into account (e.g. in trend analysis studies). Although OMI is affected by degradation effects, we were able to successfully suppress these effects by using Earthshine reference spectra. Furthermore, the data set is based on a retrieval in the visible blue spectral range, where a similar sensitivity for the near-surface layers over ocean and land is given and thus a consistent global data set can be obtained from measurements of only one sensor.

In the future, we plan to complement the data set with TCWV measurements from TROPOMI to ensure the continuation of the data set after the end of the OMI mission. Since the TCWV retrieval can be easily applied to other UV-vis satellite instruments, additional data sets from other instruments from past and present missions such as GOME-1/2 and SCIAMACHY, but also to future instruments such as Sentinel-5 on MetOp-SG can be created and eventually combined with the OMI TCWV data set taking into account the different instrumental properties (e.g. observation time). This would allow the construction of a data record that extends from 1995 to today. Similarly, a combination of data from low-earth orbit satellites and geostationary satellite instruments such as GEMS, TEMPO or Sentinel-4 could be a promising option to fill temporal gaps in daily observations, but also to investigate (semi-) diurnal cycles of the water vapour distribution.

7 Data availability

The MPIC OMI total column water vapour (TCWV) climate data record is available at https://doi.org/10.5281/zenodo.5776718 (Borger et al., 2021).

Author contributions. CB performed all calculations for this work and prepared the manuscript together with SB and TW. TW supervised this study.

Competing interests. The authors declare that they have no conflict of interest.

Acknowledgements. The combined microwave and near-infrared imager based product COMBI was initiated, funded and provided by the Water Vapour project of the ESA Climate Change Initiative, with contributions from Brockmann Consult, Spectral Earth, Deutscher Wetterdienst and the EUMETSAT Satellite Climate Facility on Climate Monitoring (CM SAF). The combined MW and NIR product will be owned by EUMETSAT CM SAFand will be released by CM SAF in late 2021. . In particular, we would like to thank Marc Schröder and the ESA CCI WV team for providing the CDR TCWV and common mask data.

Appendix A: Irradiance based vs. Earthshine SCD

To reduce the across-track biases of the retrieved H_2O SCDs based on a solar reference spectrum, a destriping algorithm can be performed during post-processing. For instance, one way to destripe the swath of an OMI orbit is to

1. calculate the median SCD for each OMI row along-track,
2. calculate the across-track median SCD from the along-track median SCDs,
3. calculate the deviation of the along-track median SCDs from this across-track median SCD,
4. subtract the deviation from the SCDs of the respective OMI row.

For the case of an Earthshine reference this is already implictly accounted for during the spectral analysis, however, one still has to consider that the Earthshine reference spectrum is not perfectly pristine of the trace gas of interest. For example in our case, although the water vapour concentrations in Antarctica are very low, the Earthshine reference might still be contaminated because of the long light path at such high solar zenith angles.

Figure A1 illustrates the time series of the global monthly mean H_2O SCDs derived from the annual-mean solar irradiance (and destriped following the aforementioned destriping process) and the Earthshine reference for SZA < 80°. Until 2009 the offset between both SCDs remains constant at values around 0.2×10^{23} molec cm^{-2}. Between 2009 and 2015 the irradiance based SCDs first decrease and then increase distinctively compared to the Earthshine based SCDs and from 2015 onwards a strong increase in the irradiance based SCDs can be observed. In contrast, the Earthshine SCDs show no jumps or steps and remain at the same magnitude after 2015 and over the complete time range in general.

To get an overview of how the SCD difference (i.e. solar irradiance based minus Earthshine SCD) behaves with time over the complete OMI swath, Fig. A2 depicts the monthly mean SCD difference for each OMI row. Between 2005 and 2009 the SCD differences remain quite constant for each row, however, after 2009 artefacts arise first at rows 55-60 and then start to expand to other rows and become even stronger. This clearly illustrates that a OMI TCWV product based on a solar irradiance fit cannot be used for trend analyses.

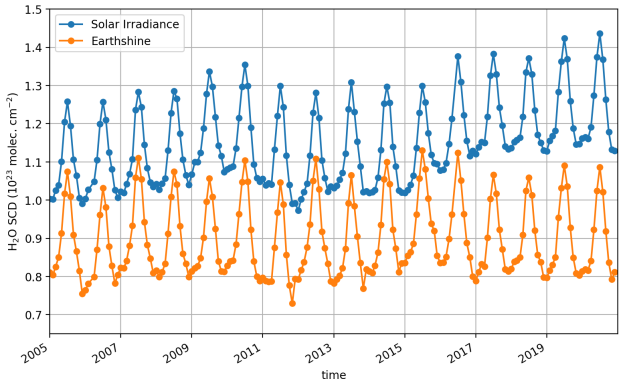

Figure A1. Globally averaged monthly-mean of the destriped H_2O SCDs derived from annual-mean solar irradiance and H_2O SCDs derived using the annual Earthshine reference from 2005 until 2020.

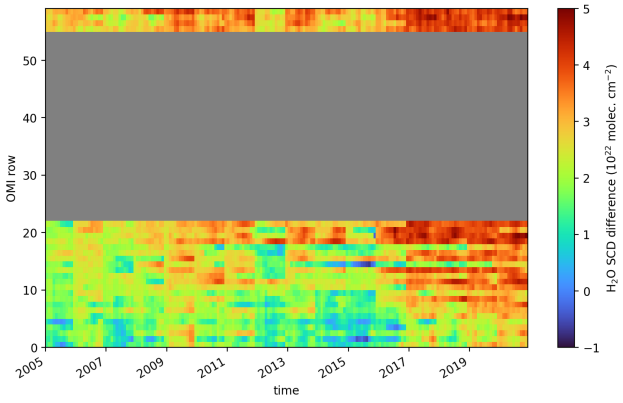

Figure A2. Global mean monthly averaged difference between annual-mean irradiance and Earthshine H_2O SCD for each OMI row separately. Only observations with a solar zenith angle $< 80^{\circ}$ and which are snow- and ice-free are included. Rows affected by the "row-anomaly" (coloured in grey) are excluded for the complete time series.

Appendix B: Validation Intercomparisons taking into account the common mask from ESA WV CCI CDR_cci

The validation intercomparison in Sect. 4 also takes into account considers regions for which only a small number of measurements are available, for example due to frequent cloud cover or seasonality of the solar zenith angle. On the one hand the small sample size of measurements leads to a higher statistical uncertainty with regard to the monthly mean, and on the other hand also to a non-continuous time series when data are missing for the complete month. Moreover, the errors of the individual measurements are also significantly larger in these regions. With the help of the "common-mask" of the ESA WV CCI _cci CDR-2 (see Fig. B1), these regions can be identified and filtered for additional validationintercomparisons.

The results of the validation intercomparisons with the "filtered" data are shown in Fig. B2 for data over ocean and in Fig. B3 for data over land. For all comparisons, the correlation coefficients remain approximately at at approximately a similar level (i.e. over above 0.95) as for the non-"filtered" comparisoncomparisons. For the comparison over ocean we obtain a slight improvement, so that overall the slopes are closer to unitycomparisons over ocean hardly any changes are obtained, as the filter is mainly applied over land surfaces. However, there is a remarkable improvement for the comparison over land: instead of a distinctive overestimation of 8-14%, the slopes now vary between 0.95 and 1.04, but this is also associated with an increase in the y-axis intercept. Altogetheralthough the fit results of the ODR change only slightly, the extreme overestimates at high TCWV values are now filtered out and the distributions are now closer to the 1-1 diagonal. Overall, the results for the "filtered" comparison over land also agree very well to findings of piecewise-linear with the results of the piecewise linear regression, for which similar regression results in the slope slope regression results were found for TCWV < 26 kg m^{-2}25 kg m^{-2}.

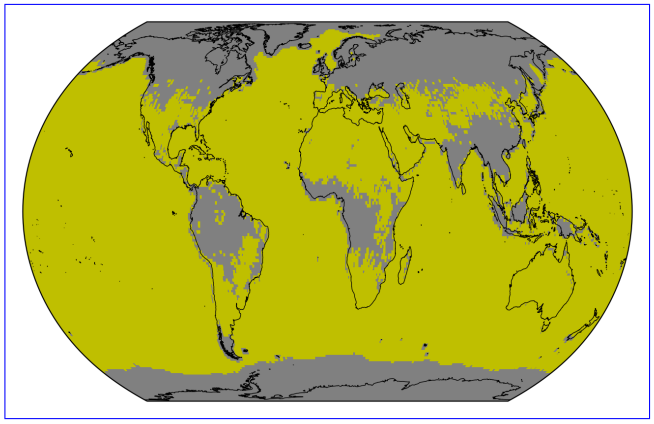

Figure B1. "Common mask" of the ESA WV CCI CDR-2. Yellow grid cells indicate data points which are accounted for within a temporal stability analysis. Invalid grid cells are coloured grey.

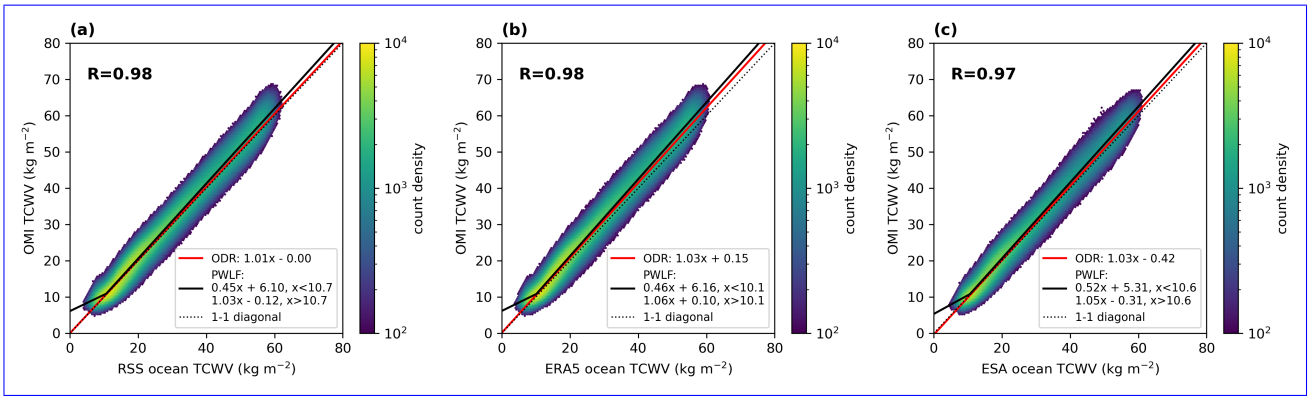

Figure B2. Correlation analysis of the OMI TCWV data set and RSS SSM/I, ERA5, the ESA WV CCI CDR-2 for data over ocean taking into account only valid grid cells according to "common mask" in Figure B1.

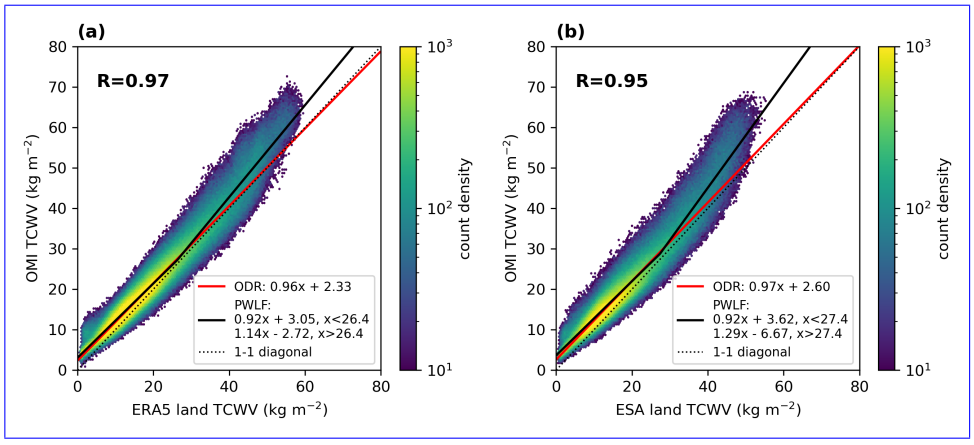

Figure B3. Same as Fig. B2, but for data over land.

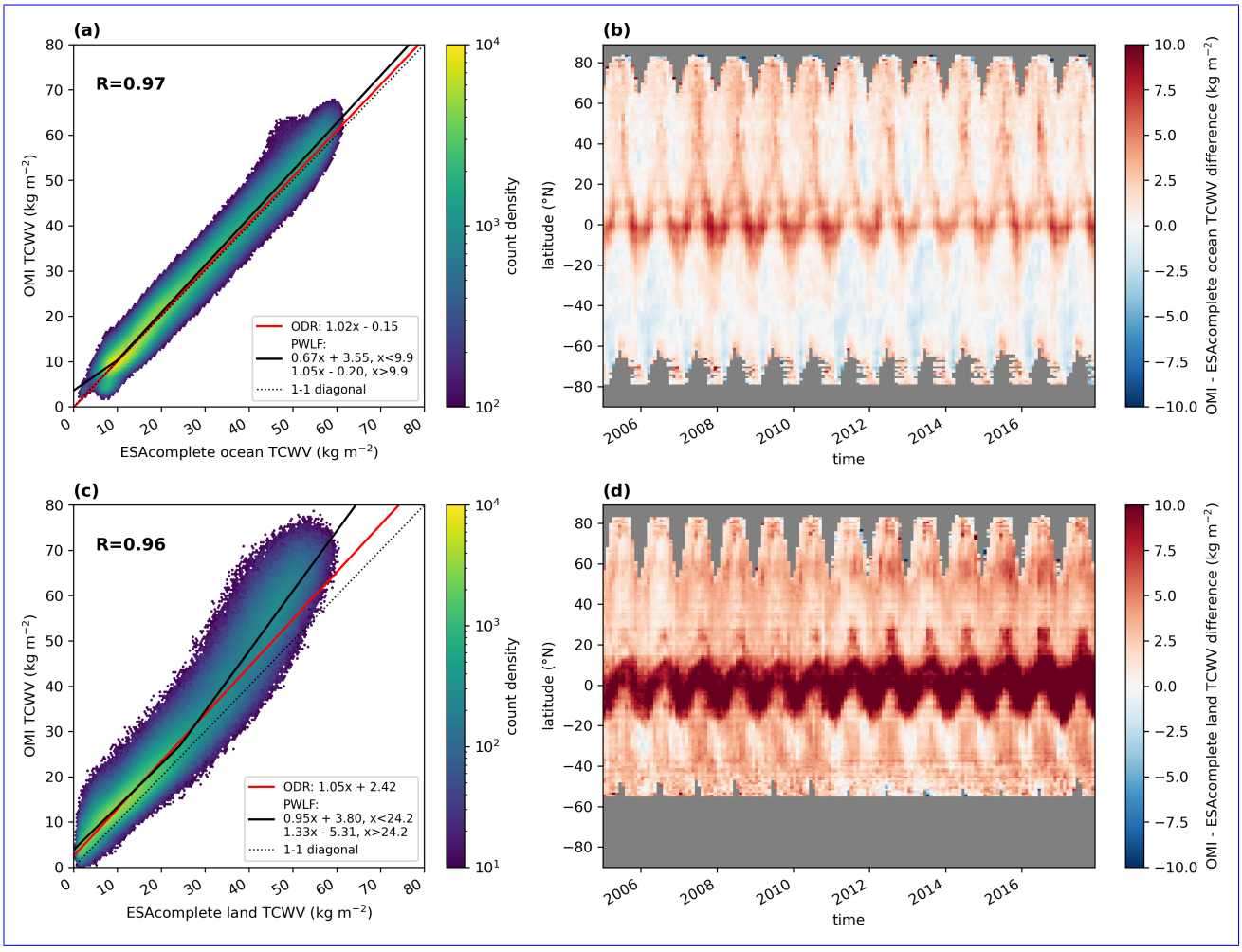

Figure B4. Same as Fig. 11, but now with ESA WV CCI CDR-2 data for data over ocean (top row) and for data over land (bottom row) for the complete time range.

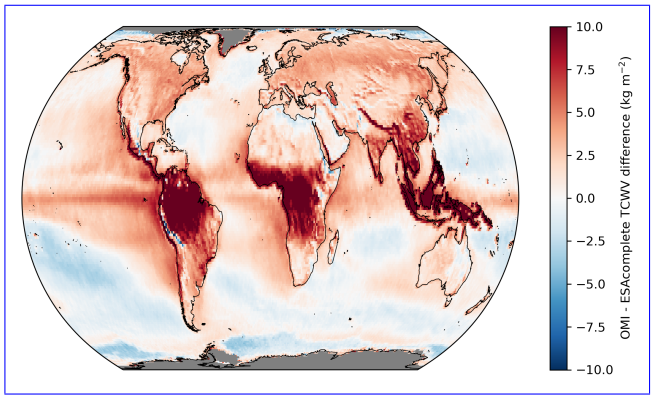

Figure B5. Same as Fig.12, but now for ESA WV CCI CDR data over the complete time range.

Appendix C: Representativeness of row-anomaly filtered data in comparison to full swath

Due to the row anomaly filter, approximately 50% of the complete satellite swath of OMI is not considered in the TCWV data set. This raises the question of how much the monthly mean values would differ if the data of the complete swath were available. To investigate this, we follow the same scheme as in Sect. 3 and use the same ERA5 data as a reference. We select the ERA5 data to match the OMI overpass, once applying the row-anomaly filter and once not. However, in both cases the clear-sky filter based on the OMI cloud information is applied (effective cloud fraction < 20%).

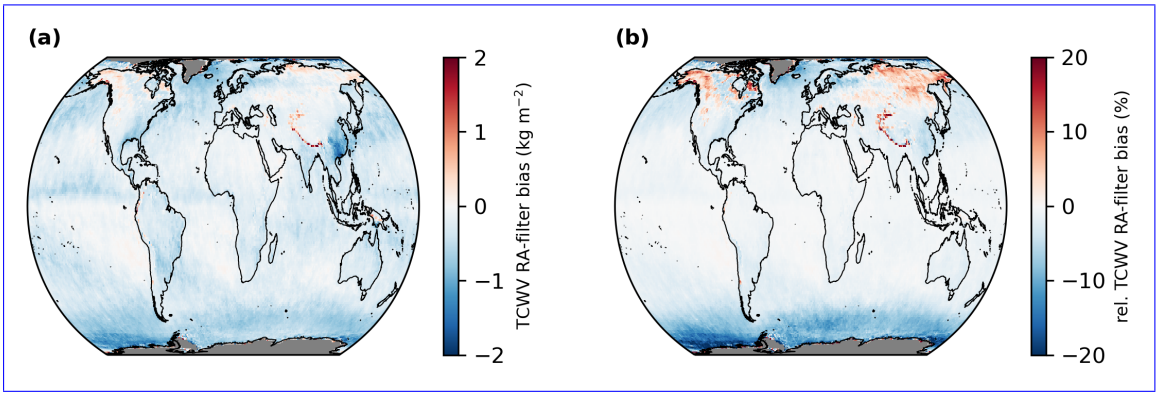

Figure C1. Global distributions of the mean differences between row-anomaly (RA) filtered and full swath ERA5 based on the OMI cloud information for the time range January 2005 to December 2020. Panel (a) depicts the absolute differences (i.e. RA-filtered minus full swath) and Panel (b) relative differences (i.e. (RA-filtered minus full swath) / full swath). Grid cells for which no data is available are coloured grey.

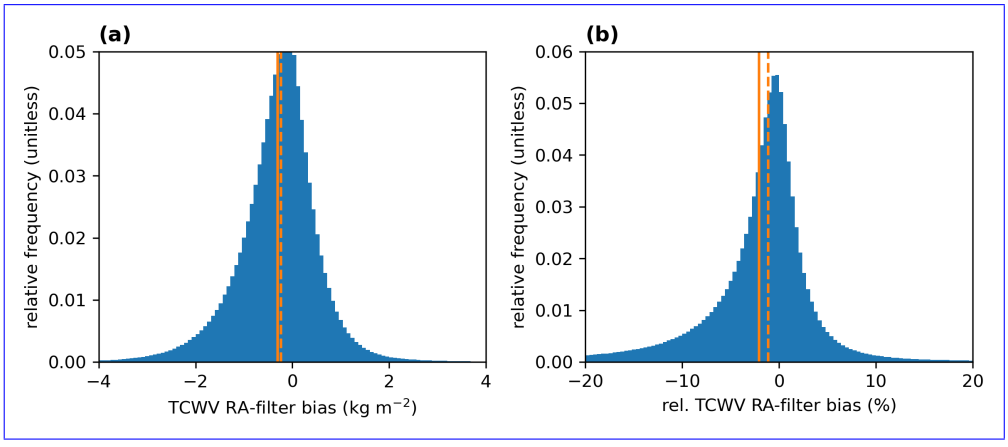

Figure C2. Distributions of the absolute differences (RA-filtered minus full swath; Panel a) and relative differences ((RA-filtered minus full swath) / full swath; Panel b) of the monthly mean differences between RA-filtered and full swath ERA5 data based on the OMI cloud information. The solid and dashred orange line indicate the mean and the median of the distributions, respectively.

Compared to the clear-sky bias, the deviations are much weaker and no particular spatial patterns are discernible in the global distributions except in the deep Pacific tropics and parts of Southeast Asia (see Fig. C1). Furthermore, the histograms for the absolute and relative deviations in Fig. C2 show a normal distribution for both cases with mean values of $-0.30\,\mathrm{kg\,m^{-2}}$ and -2.1% (and for the median $-0.23\,\mathrm{kg\,m^{-2}}$ and -1.1%). Considering the much larger uncertainties of the OMI TCWV retrievals of typically 20% and more and that the clear-sky bias is almost one order of magnitude larger, the obtained deviations are negligible and thus the monthly means from the RA-filtered data are a good representation compared to the monthly means from the data for a full swath, even though only half of the satellite data is actually used.

References

Anand, J. S., Monks, P. S., and Leigh, R. J.: An improved retrieval of tropospheric NO_2 from space over polluted regions using an Earth radiance reference, Atmospheric Measurement Techniques, 8, 1519–1535, https://doi.org/10.5194/amt-8-1519-2015, 2015.

Beirle, S., Lampel, J., Wang, Y., Mies, K., Dörner, S., Grossi, M., Loyola, D., Dehn, A., Danielczok, A., Schröder, M., and Wagner, T.: The ESA GOME-Evolution "Climate" water vapor product: a homogenized time series of H_2O columns from GOME, SCIAMACHY, and GOME-2, Earth System Science Data, 10, 449–468, https://doi.org/10.5194/essd-10-449-2018, 2018.

Bennartz, R. and Fischer, J.: Retrieval of columnar water vapour over land from backscattered solar radiation using the Medium Resolution Imaging Spectrometer, Remote Sensing of Environment, 78, 274–283, https://doi.org/10.1016/S0034-4257(01)00218-8, 2001.

Boersma, K. F., Eskes, H. J., Richter, A., De Smedt, I., Lorente, A., Beirle, S., van Geffen, J. H. G. M., Zara, M., Peters, E., Van Roozendael, M., Wagner, T., Maasakkers, J. D., van der A, R. J., Nightingale, J., De Rudder, A., Irie, H., Pinardi, G., Lambert, J.-C., and Compernolle, S. C.: Improving algorithms and uncertainty estimates for satellite NO_2 retrievals: results from the quality assurance for the essential climate variables (QA4ECV) project, Atmospheric Measurement Techniques, 11, 6651–6678, https://doi.org/10.5194/amt-11-6651-2018, 2018.

Borger, C., Beirle, S., Dörner, S., Sihler, H., and Wagner, T.: Total column water vapour retrieval from S-5P/TROPOMI in the visible blue spectral range, Atmospheric Measurement Techniques, 13, 2751–2783, https://doi.org/10.5194/amt-13-2751-2020, 2020.

Borger, C., Beirle, S., and Wagner, T.: MPIC OMI Total Column Water Vapour (TCWV) Climate Data Record, https://doi.org/10.5281/zenodo.5776718, 2021.

Borger, C., Beirle, S., and Wagner, T.: Analysis of global trends of total column water vapour from multiple years of OMI observations, Atmospheric Chemistry and Physics Discussions, 2022, 1–27, https://doi.org/10.5194/acp-2022-149, 2022.

Cantrell, C. A.: Technical Note: Review of methods for linear least-squares fitting of data and application to atmospheric chemistry problems, Atmospheric Chemistry and Physics, 8, 5477–5487, https://doi.org/10.5194/acp-8-5477-2008, 2008.

Chan, K. L., Valks, P., Slijkhuis, S., Köhler, C., and Loyola, D.: Total column water vapor retrieval for Global Ozone Monitoring Experience-2 (GOME-2) visible blue observations, Atmospheric Measurement Techniques, 13, 4169–4193, https://doi.org/10.5194/amt-13-4169-2020, 2020.

Danielczok, A. and Schröder, M.: GOME Evolution "Climate" product validation report, resreport, European Space Agency, https://earth.esa.int/documents/700255/1525725/GOME_EVL_L3_ValRep_final/db7e72c3-044d-4236-9dee-d88405b89ef0, 2017.

Danne, O., Falk, U., Preusker, R., Brockmann, C., Fischer, J., Hegglin, M., and Schröder, M.: ESA Water Vapour Climate Change Initiative (Water_Vapour_cci): Total Column Water Vapour monthly gridded data over land at 0.5 degree resolution, version 3.2, NERC EDS Centre for Environmental Data Analysis, https://doi.org/10.5285/4a85c0ef880e4f668cd4ec8e846855ef, 2022.

Dupuy, E., Morino, I., Deutscher, N. M., Yoshida, Y., Uchino, O., Connor, B. J., De Mazière, M., Griffith, D. W. T., Hase, F., Heikkinen, P., Hillyard, P. W., Iraci, L. T., Kawakami, S., Kivi, R., Matsunaga, T., Notholt, J., Petri, C., Podolske, J. R., Pollard, D. F., Rettinger, M., Roehl, C. M., Sherlock, V., Sussmann, R., Toon, G. C., Velazco, V. A., Warneke, T., Wennberg, P. O., Wunch, D., and Yokota, T.: Comparison of XH2O Retrieved from GOSAT Short-Wavelength Infrared Spectra with Observations from the TCCON Network, Remote Sensing, 8, https://doi.org/10.3390/rs8050414, 2016.

Fennig, K., Schröder, M., Andersson, A., and Hollmann, R.: A Fundamental Climate Data Record of SMMR, SSM/I, and SSMIS brightness temperatures, Earth System Science Data, 12, 647–681, https://doi.org/10.5194/essd-12-647-2020, 2020.

Gaffen, D. J. and Elliott, W. P.: Column Water Vapor Content in Clear and Cloudy Skies, Journal of Climate, 6, 2278 – 2287, https://doi.org/10.1175/1520-0442(1993)006<2278:CWVCIC>2.0.CO;2, 1993.

Gao, B.-C. and Kaufman, Y. J.: Water vapor retrievals using Moderate Resolution Imaging Spectroradiometer (MODIS) near-infrared channels, Journal of Geophysical Research: Atmospheres, 108, https://doi.org/10.1029/2002JD003023, 2003.

Gleisner, H., Lauritsen, K. B., Nielsen, J. K., and Syndergaard, S.: Evaluation of the 15-year ROM SAF monthly mean GPS radio occultation climate data record, Atmospheric Measurement Techniques, 13, 3081–3098, https://doi.org/10.5194/amt-13-3081-2020, 2020.

Grossi, M., Valks, P., Loyola, D., Aberle, B., Slijkhuis, S., Wagner, T., Beirle, S., and Lang, R.: Total column water vapour measurements from GOME-2 MetOp-A and MetOp-B, Atmospheric Measurement Techniques, 8, 1111–1133, https://doi.org/10.5194/amt-8-1111-2015, 2015.

Held, I. M. and Soden, B. J.: Water Vapor Feedback and Global Warming, Annual Review of Energy and the Environment, 25, 441–475, https://doi.org/10.1146/annurev.energy.25.1.441, 2000.

Hersbach, H., Bell, B., Berrisford, P., Biavati, G., Horányi, A., Muñoz Sabater, J., Nicolas, J., Peubey, C., Radu, R., Rozum, I., Schepers, D., Simmons, A., Soci, C., Dee, D., and Thépaut, J.-N.: ERA5 monthly averaged data on single levels from 1979 to present, Copernicus Climate Change Service (C3S) Climate Data Store (CDS), https://doi.org/10.24381/cds.f17050d7, (Accessed on: 2021-07-01), 2019.

Hersbach, H., Bell, B., Berrisford, P., Hirahara, S., Horányi, A., Muñoz-Sabater, J., Nicolas, J., Peubey, C., Radu, R., Schepers, D., Simmons, A., Soci, C., Abdalla, S., Abellan, X., Balsamo, G., Bechtold, P., Biavati, G., Bidlot, J., Bonavita, M., De Chiara, G., Dahlgren, P., Dee, D., Diamantakis, M., Dragani, R., Flemming, J., Forbes, R., Fuentes, M., Geer, A., Haimberger, L., Healy, S., Hogan, R. J., Hólm, E., Janisková, M., Keeley, S., Laloyaux, P., Lopez, P., Lupu, C., Radnoti, G., de Rosnay, P., Rozum, I., Vamborg, F., Villaume, S., and Thépaut, J.-N.: The ERA5 global reanalysis, Quarterly Journal of the Royal Meteorological Society, 146, 1999–2049, https://doi.org/10.1002/qj.3803, 2020.

Kiehl, J. T. and Trenberth, K. E.: Earth's Annual Global Mean Energy Budget., Bulletin of the American Meteorological Society, 78, 197–197, https://doi.org/10.1175/1520-0477(1997)078<0197:EAGMEB>2.0.CO;2, 1997.

Kleipool, Q. L., Dobber, M. R., de Haan, J. F., and Levelt, P. F.: Earth surface reflectance climatology from 3 years of OMI data, Journal of Geophysical Research: Atmospheres, 113, https://doi.org/10.1029/2008JD010290, 2008.

Koelemeijer, R. B. A., de Haan, J. F., and Stammes, P.: A database of spectral surface reflectivity in the range 335–772 nm derived from 5.5 years of GOME observations, Journal of Geophysical Research: Atmospheres, 108, https://doi.org/https://doi.org/10.1029/2002JD002429, 2003.

Kursinski, E. R., Hajj, G. A., Schofield, J. T., Linfield, R. P., and Hardy, K. R.: Observing Earth's atmosphere with radio occultation measurements using the Global Positioning System, Journal of Geophysical Research: Atmospheres, 102, 23 429–23 465, https://doi.org/10.1029/97JD01569, 1997.

Lamsal, L. N., Krotkov, N. A., Vasilkov, A., Marchenko, S., Qin, W., Yang, E.-S., Fasnacht, Z., Joiner, J., Choi, S., Haffner, D., Swartz, W. H., Fisher, B., and Bucsela, E.: Ozone Monitoring Instrument (OMI) Aura nitrogen dioxide standard product version 4.0 with improved surface and cloud treatments, Atmospheric Measurement Techniques, 14, 455–479, https://doi.org/10.5194/amt-14-455-2021, 2021.

Lang, R., Williams, J. E., van der Zande, W. J., and Maurellis, A. N.: Application of the Spectral Structure Parameterization technique: retrieval of total water vapor columns from GOME, Atmospheric Chemistry and Physics, 3, 145–160, https://doi.org/10.5194/acp-3-145-2003, 2003.

Levelt, P. F., van den Oord, G. H., Dobber, M. R., Malkki, A., Visser, H., de Vries, J., Stammes, P., Lundell, J. O., and Saari, H.: The ozone monitoring instrument, IEEE Transactions on Geoscience and Remote Sensing, 44, 1093–1101, https://doi.org/10.1109/TGRS.2006.872333, 2006.

Levelt, P. F., Joiner, J., Tamminen, J., Veefkind, J. P., Bhartia, P. K., Stein Zweers, D. C., Duncan, B. N., Streets, D. G., Eskes, H., van der A, R., McLinden, C., Fioletov, V., Carn, S., de Laat, J., DeLand, M., Marchenko, S., McPeters, R., Ziemke, J., Fu, D., Liu, X., Pickering, K., Apituley, A., González Abad, G., Arola, A., Boersma, F., Chan Miller, C., Chance, K., de Graaf, M., Hakkarainen, J., Hassinen, S., Ialongo, I., Kleipool, Q., Krotkov, N., Li, C., Lamsal, L., Newman, P., Nowlan, C., Suleiman, R., Tilstra, L. G., Torres, O., Wang, H., and Wargan, K.: The Ozone Monitoring Instrument: overview of 14 years in space, Atmospheric Chemistry and Physics, 18, 5699–5745, https://doi.org/10.5194/acp-18-5699-2018, 2018.

Li, J., Wang, P., Han, H., Li, J., and Zheng, J.: On the assimilation of satellite sounder data in cloudy skies in numerical weather prediction models, Journal of Meteorological Research, 30, 169–182, https://doi.org/10.1007/s13351-016-5114-2, 2016.

Mears, C. A., Wang, J., Smith, D., and Wentz, F. J.: Intercomparison of total precipitable water measurements made by satellite-borne microwave radiometers and ground-based GPS instruments, Journal of Geophysical Research: Atmospheres, 120, 2492–2504, https://doi.org/10.1002/2014JD022694, 2015.

Munro, R., Lang, R., Klaes, D., Poli, G., Retscher, C., Lindstrot, R., Huckle, R., Lacan, A., Grzegorski, M., Holdak, A., Kokhanovsky, A., Livschitz, J., and Eisinger, M.: The GOME-2 instrument on the Metop series of satellites: instrument design, calibration, and level 1 data processing – an overview, Atmospheric Measurement Techniques, 9, 1279–1301, https://doi.org/10.5194/amt-9-1279-2016, 2016.

Noël, S., Buchwitz, M., Bovensmann, H., Hoogen, R., and Burrows, J. P.: Atmospheric water vapor amounts retrieved from GOME satellite data, Geophysical Research Letters, 26, 1841–1844, https://doi.org/10.1029/1999GL900437, 1999.

Platt, U. and Stutz, J.: Differential Optical Absorption Spectroscopy: Principles and Applications, Physics of Earth and Space Environments, Springer Berlin Heidelberg, https://doi.org/10.1007/978-3-540-75776-4, 2008.

Randall, D. A., Wood, R. A., Bony, S., Colman, R., Fichefet, T., Fyfe, J., Kattsov, V., Pitman, A., Shukla, J., Srinivasan, J., et al.: Climate models and their evaluation, in: Climate change 2007: The physical science basis. Contribution of Working Group I to the Fourth Assessment Report of the IPCC (FAR), pp. 589–662, Cambridge University Press, 2007.

Rosenkranz, P. W.: Retrieval of temperature and moisture profiles from AMSU-A and AMSU-B measurements, IEEE Transactions on Geoscience and Remote Sensing, 39, 2429–2435, https://doi.org/10.1109/36.964979, 2001.

Schenkeveld, V. M. E., Jaross, G., Marchenko, S., Haffner, D., Kleipool, Q. L., Rozemeijer, N. C., Veefkind, J. P., and Levelt, P. F.: In-flight performance of the Ozone Monitoring Instrument, Atmospheric Measurement Techniques, 10, 1957–1986, https://doi.org/10.5194/amt-10-1957-2017, 2017.

Schlüssel, P., Hultberg, T. H., Phillips, P. L., August, T., and Calbet, X.: The operational IASI Level 2 processor, Advances in Space Research, 36, 982–988, https://doi.org/10.1016/j.asr.2005.03.008, atmospheric Remote Sensing: Earth's Surface, Troposphere, Stratosphere and Mesosphere- I, 2005.

Schneider, A., Borsdorff, T., aan de Brugh, J., Aemisegger, F., Feist, D. G., Kivi, R., Hase, F., Schneider, M., and Landgraf, J.: First data set of H_2O/HDO columns from the Tropospheric Monitoring Instrument (TROPOMI), Atmospheric Measurement Techniques, 13, 85–100, https://doi.org/10.5194/amt-13-85-2020, 2020.

Schneider, M. and Hase, F.: Optimal estimation of tropospheric H_2O and δD with IASI/METOP, Atmospheric Chemistry and Physics, 11, 11 207–11 220, https://doi.org/10.5194/acp-11-11207-2011, 2011.

Schrijver, H., Gloudemans, A. M. S., Frankenberg, C., and Aben, I.: Water vapour total columns from SCIAMACHY spectra in the 2.36 µm window, Atmospheric Measurement Techniques, 2, 561–571, https://doi.org/10.5194/amt-2-561-2009, 2009.

Sohn, B.-J. and Bennartz, R.: Contribution of water vapor to observational estimates of longwave cloud radiative forcing, Journal of Geophysical Research: Atmospheres, 113, https://doi.org/10.1029/2008JD010053, 2008.

Stevens, B. and Bony, S.: What Are Climate Models Missing?, Science, 340, 1053–1054, https://doi.org/10.1126/science.1237554, 2013.

Sulla-Menashe, D., Gray, J. M., Abercrombie, S. P., and Friedl, M. A.: Hierarchical mapping of annual global land cover 2001 to present: The MODIS Collection 6 Land Cover product, Remote Sensing of Environment, 222, 183 – 194, https://doi.org/10.1016/j.rse.2018.12.013, 2019.

Susskind, J., Barnet, C., and Blaisdell, J.: Retrieval of atmospheric and surface parameters from AIRS/AMSU/HSB data in the presence of clouds, IEEE Transactions on Geoscience and Remote Sensing, 41, 390–409, https://doi.org/10.1109/TGRS.2002.808236, 2003.

Tilstra, L. G., Tuinder, O. N. E., Wang, P., and Stammes, P.: Surface reflectivity climatologies from UV to NIR determined from Earth observations by GOME-2 and SCIAMACHY, Journal of Geophysical Research: Atmospheres, 122, 4084–4111, https://doi.org/10.1002/2016JD025940, 2017.

Trenberth, K. E., Fasullo, J. T., and Kiehl, J.: Earth's Global Energy Budget, Bulletin of the American Meteorological Society, 90, 311 – 324, https://doi.org/10.1175/2008BAMS2634.1, 2009.

Veefkind, J., Aben, I., McMullan, K., Förster, H., de Vries, J., Otter, G., Claas, J., Eskes, H., de Haan, J., Kleipool, Q., van Weele, M., Hasekamp, O., Hoogeveen, R., Landgraf, J., Snel, R., Tol, P., Ingmann, P., Voors, R., Kruizinga, B., Vink, R., Visser, H., and Levelt, P.: TROPOMI on the ESA Sentinel-5 Precursor: A GMES mission for global observations of the atmospheric composition for climate, air quality and ozone layer applications, Remote Sensing of Environment, 120, 70 – 83, https://doi.org/10.1016/j.rse.2011.09.027, the Sentinel Missions - New Opportunities for Science, 2012.

Wagner, T., Heland, J., Zöger, M., and Platt, U.: A fast H_2O total column density product from GOME - Validation with in-situ aircraft measurements, Atmospheric Chemistry and Physics, 3, 651–663, https://doi.org/10.5194/acp-3-651-2003, 2003.

Wagner, T., Beirle, S., Sihler, H., and Mies, K.: A feasibility study for the retrieval of the total column precipitable water vapour from satellite observations in the blue spectral range, Atmospheric Measurement Techniques, 6, 2593–2605, https://doi.org/10.5194/amt-6-2593-2013, 2013.

Wang, H., Souri, A. H., González Abad, G., Liu, X., and Chance, K.: Ozone Monitoring Instrument (OMI) Total Column Water Vapor version 4 validation and applications, Atmospheric Measurement Techniques, 12, 5183–5199, https://doi.org/10.5194/amt-12-5183-2019, 2019.

Wentz, F. J.: A 17-Yr Climate Record of Environmental Parameters Derived from the Tropical Rainfall Measuring Mission (TRMM) Microwave Imager, Journal of Climate, 28, 6882 – 6902, https://doi.org/10.1175/JCLI-D-15-0155.1, 2015.

Xue, Y., Li, J., Menzel, W. P., Borbas, E., Ho, S.-P., Li, Z., and Li, J.: Characteristics of Satellite Sampling Errors in Total Precipitable Water from SSMIS, HIRS, and COSMIC Observations, Journal of Geophysical Research: Atmospheres, 124, 6966–6981, https://doi.org/https://doi.org/10.1029/2018JD030045, 2019.